Fall 1-31-2004

Dielectrophoretic manipulation of biological and non-biological analytes in a microfluidic channel

Dawn J. Bennett
New Jersey Institute of Technology

Recommended Citation

Bennett, Dawn J., "Dielectrophoretic manipulation of biological and non-biological analytes in a microfluidic channel" (2004). *Dissertations*. 600.
https://digitalcommons.njit.edu/dissertations/600

ABSTRACT

DIELECTROPHORETIC MANIPULATION OF BIOLOGICAL AND NON-BIOLOGICAL ANALYTES IN A MICROFLUIDIC CHANNEL

by

Dawn J. Bennett

Micro-total-analytical systems (μTAS s) for analyzing chemical/biological substances are now used across a wide variety of applications ranging from biological warfare agent detection to the healthcare industry. The first step in the operation of a μTAS consists of concentrating and separating the analytes of interest from the background matrix and positioning them into selected locations for subsequent analysis. The use of ac electric fields was demonstrated to have promising potential for a μTAS because the application of an ac field suppresses undesirable electrolytic effects in the liquid. The main purpose of this work is to study micro-scale phenomena in a flowing suspension subject to shear and high-gradient strong ac electric field.

A microfluidic device equipped with dielectrophoretic gates arranged perpendicular to the flow was designed and fabricated at Sandia National Laboratories. Experiments were conducted on flowing suspensions over a broad range of flow and electric field parameters to investigate how these characteristics affect the concentration and separation of particles. It was found that dipolar interactions between suspended particles subject to a high-gradient ac field and shear lead to a new many-body phenomenon of dielectrophoresis accompanied by the field-induced phase separation in a flowing suspension. As

a result, shear and electric stresses strongly compress a layer enriched with particles. The predictions of the proposed electro-hydrodynamic model for the coupled shear, dielectrophoresis, and phase separation in a flowing suspension are shown to be consistent with experimental data even though the model contains no fitting parameters. Both the model and the experiments showed that the concentration volume could be increased up to about 50%. It was demonstrated that the field-induced dielectrophoresis accompanied by the phase separation provides a new method for concentrating particles in focused regions and for separating biological and non-biological materials, a critical step in the development of miniaturizing biological assays. Specifically, experiments were performed using 1 μm diameter polystyrene latex beads and heat-killed (Staphylococcus aureus; Molecular probes) dispersed in deionized water.

DIELECTROPHORETIC MANIPULATION OF BIOLOGICAL AND NON-BIOLOGICAL ANALYTES IN A MICROFLUIDIC CHANNEL

by

Dawn J. Bennett

A Dissertation
Submitted to the Faculty of
New Jersey Institute of Technology
In Partial Fulfillment of the Requirements for the Degree of
Doctor of Philosophy in Mechanical Engineering

Department of Mechanical Engineering

January 2004

APPROVAL PAGE

DIELECTROPHORETIC MANIPULATION OF BIOLOGICAL AND NON-BIOLOGICAL ANALYTES IN A MICROFLUIDIC CHANNEL

Dawn Jonita Bennett

Dr. Boris Khusid, Dissertation Advisor — Date
Associate Professor of Mechanical Engineering, NJIT

Dr. Paul Galambos, Dissertation Advisor — Date
Member of Technical Staff, Sandia National Laboratories, Albuquerque, NM

Dr. Edward L. Dreizin, Committee Member — Date
Associate Professor of Mechanical Engineering, NJIT

Dr. Ernest S. Geskin, Committee Member — Date
Professor of Mechanical Engineering, NJIT

Dr. Kenneth R. Farmer, Committee Member — Date
Associate Professor of Physics, NJIT

Dr. Avraham Harnoy, Committee Member — Date
Professor of Mechanical Engineering, NJIT

BIOGRAPHICAL SKETCH

Author: Dawn J. Bennett

Degree: Doctor of Philosophy

Date: January 2004

Undergraduate and Graduate Education:

- Doctor of Philosophy in Mechanical Engineering,
  New Jersey Institute of Technology, Newark, NJ, (January, 2004)

- Master of Science in Mechanical Engineering,
  Duke University, Durham, North Carolina, 1990

- Bachelor of Science in Mechanical Engineering
  Brown University, Providence, RI, 1988

Major: Mechanical Engineering

Presentations

D. Bennett, B. Khusid, P. Galambos, C. D. James, M. Okandan, D. Jacqmin, A. Acrivos, Combined Field-induced Dielectrophoresis and Phase Separation for Manipulating Particles in Microfluidics, American Physical Society, Division of Fluid Dynamics 56th Annual Meeting, East Rutherford, NJ, November 23-25, 2003.

D. Bennett, B. Khusid, P. Galambos, C. D. James, M. Okandan, D. Jacqmin, A. Acrivos, A Dielectrophoretic Particle and Cell Concentrator, ASME International Mechanical Engineering Congress, Washington, DC, November 15-21, 2003.

D. Bennett, B. Khusid, P. Galambos, C. D. James, M. Okandan, A Dielectrophoretic Particle Concentrator, Transducers '03: The 12th International Conference on Solid-State Sensors, Actuators and Microsystems, Boston, MA, June 8-12, 2003.

D. Bennett, B. Khusid, P. Galambos, C. D. James, M. Okandan, A Dielectrophoretic Particle and Cell Concentrator, The National Society of Black Engineers, 29th National Convention, Anaheim, CA, March 19-23, 2003.

D. Bennett, B. Khusid, P. Galambos, M. Okandan, Manipulation of Particles in Fluids Using a Microfluidics Channel System Involving Both Traditional and Travelling Wave Dielectrophoresis- Analysis and Design, Fourteenth U.S. National Congress of Theoretical and Applied Mechanics, Blacksburg Virginia, June 2002.

D. Bennett, B. Khusid, P. Galambos, M. Okandan, Manipulation of Particles in Microfluidic Channels by Means of Travelling Wave Dielectrophoresis, Student Symposium, Albuquerque, New Mexico, June 2002.

D. Bennett, B. Khusid, P. Galambos, C. D. James, M. Okandan , Manipulation of Particles in Fluids Using a Microfluidics Channel System by means of Conventional and Travelling Wave Dielectrophoresis, ASME International Mechanical Engineering Congress, New Orleans, Louisiana, November 2002.

D. Bennett, B. Khusid, P. Galambos, M. Okandan, Manipulation of Particles in Microfluidic Channels, Micromachining Project and Technology Status Meeting, Albuquerque, New Mexico, May, 2002.

D. Bennett, B. Khusid, P. Galambos, M. Okandan, The Manipulation of Particles in Fluids via Dielectrophoresis, Student Symposium, Albuquerque, New Mexico, June 2001.

Publications:

D. Bennett, B. Khusid, P. Galambos, C. D. James, M. Okandan, D. Jacqmin, A. Acrivos, Combined Field-induced Dielectrophoresis and Phase Separation for Manipulating Particles in Microfluidics, Applied Physics Letters, v. 83 (23), 2003.

D. Bennett, B. Khusid, P. Galambos, C. D. James, M. Okandan, A Dielectrophoretic Particle and Cell Concentrator, TRANSDUCERS '03 The 12th International Conference on Solid-State Sensors, Actuators and Microsystems, Boston, MA, June 8 -12, 2003, pp.1225-1228

D. Bennett, B. Khusid, P. Galambos, M. Okandan, Manipulation of Particles in a Microfluidics Channel Using and Travelling Wave Dielectrophoresis- - Design and Analysis, Contemporary Research in Theoretical and Applied Mechanics, Proceedings of Fourteenth U.S. National Congress of Theoretical and Applied Mechanics, Blacksburg Virginia, June 23-28, 2002, pp.406-407.

SUCCESS

Some people succeed because they are destined to, but most people succeed because they are determined to. -- Unknown

If you wish success in life, make perseverance your bosom friend, experience your wise counselor, caution your elder brother and hope your guardian genius.

Joseph Addison (1672 - 1719)

This dissertation is dedicated to my family and friends for their support throughout this endeavor.

ACKNOWLEDGMENT

I would like to express my sincerest appreciation to my advisors, Dr. Boris Khusid, NJIT, and Dr. Paul Galambos, SNL, for their time, support, encouragement, enthusiasm, wisdom, insightfulness, and direction. Both were outstanding advisors. Special thanks is also given to Dr. Edward Dreizin, Dr. Kenneth Farmer, Dr. Ernest Geskin, and Dr. Avraham Harnoy for actively participating on my committee.

I would also like to thank all of my colleagues at Sandia National Laboratories. I am grateful to my managers at Sandia National Laboratories, Mr. Jay Jakubczak and Dr. David Sandison, for given me the opportunity to work with excellent scientists in an extremely resourceful environment. I am extremely indebted to Dr. Conrad James for his guidance and assistance during my tenure at Sandia National Laboratories. In addition, I would like to thank Dr. Murat Okandan for the use of his designs and his assistance. Special recognition is also given to Dr. Sita Mani for her processing knowledge and direction; Mr. Kenneth Pohl for his technical assistance in the laboratory; and Dr. Len Duda for his assistance in making the permittivity measurements.

Thanks to Dr. Ronald Kane, NJIT, for financially supporting me with the NSF AGEP- MAGNET fellowship. In addition, I am grateful to Dr. Regan Stinnett, SNL, for providing support through Sandia National Laboratories' MESA Institute.

TABLE OF CONTENTS

TABLE OF CONTENTS
(Continued)

LIST OF FIGURES

LIST OF FIGURES
(Continued)

LIST OF FIGURES
(Continued)

LIST OF FIGURES
(Continued)

LIST OF FIGURES
(Continued)

LIST OF FIGURES
(Continued)

LIST OF FIGURES
(Continued)

CHAPTER 1

INTRODUCTION

1.1 Microfluidic Devices

In general, microfluidic devices refer to technologies that involve the flow of minute amounts of liquids and gases typically measured in nano- and pico-liter scales. While microelectronics emphasizes reducing the size of transistors, microfluidics focuses on the development of complex systems for more sophisticated methods of handling fluids. It has been demonstrated that microscale devices are largely superior to their macroscale analogs in certain applications. Microscale systems offer the advantages of compact size, disposability, higher speed and parallelism for analysis as well as increased functionality. Microscale devices have been shown to have unique transport properties as a result of drastically increased surface to volume ratios. They require significantly smaller sample volumes for testing which is the major advantage for situations where the reagents or analytes are dangerous or expensive. In the life sciences, in particular, the interaction of microsystems with living cells or tissues opens up the road to novel methods of medical applications, diagnostic as well as therapeutic, which highly impacts the field of BioMEMS. Conventional methods in medical technology have shifted towards the miniaturization and MEMS, especially in the areas of invasive surgery and in vivo and ex vivo monitoring and smart implants. In addition, the utility, speed, and resolution performance of microsystems typically increases as the overall size of the device decreases. (Koch et al.,2000, Terray et al., 2002). Although similar components such as valves, pumps, mixers, filters, and separators are used in both micro- and macro-scale systems, the flow behaves differently in microchannels due to their small size. Even though the fluid properties remain the same at the microscale, surface tension, viscosity, and electrical charges can become dominant forces on a fluid because the surface-to-volume ratio is much greater than for macroscale systems. In addition, it is not fully understood how heat transfer and mass transfer function at the microscale, and what effect they might have on the device (Ouellette, 2002).

Interest in microfluidics has been largely motivated by applications. The most mature microfluidic technology is ink-jet printing, which uses orifices less than 100 μm in diameter for the generation of ink drops. Ink-jet printing has been rapidly finding a place in biotechnology for the delivery of reagents to microscopic reactors and for the deposition of DNA into arrays on the surface of biochips. In particular, hand-held systems developed by I-Stat Corp for hospital-based analysis of serum electrolytes were the first commercially developed small analytical systems, which use submillimeter-sized channels. Complex devices are now being developed for a wide range of biological, medical, and biodefense applications. In general, this involves working with aqueous solutions flowing through 50-μm to 100-μm channels (Whitesides et al., 2001). Such channels require only a small amount of samples and reagents for each process as compared to roughly 100 ml required for currently available plate assays. In addition, biochemical reactions occur significantly faster because of the unique physics of small fluid volumes, and microfluidic technologies can be automated to perform routine sample and assay preparation on standard microchips without much human interaction (Ouellette, 2002, Effenhauser et al., 1993). Multiple functions can be combined on a microchip as is the case, for example, of Sandia National Laboratories μChemLab-on-a-chip, which involves a preconcentrator, separator, and detector. Microfluidic techniques are used to guide the sample from one part of the chip to another. The field of microfluidics is rapidly growing and expanding. It is facilitated by the move towards more simple and robust fabrication methods such as rapid prototyping based on molding of elastomers which reduce costs and design and fabrication cycles. Currently, there exist no industry standards for microfluidic systems, and the field remains open for exploration (Ouellette, 2002).

Several electric field-based techniques are used in microfluidic devices to manipulate fluids and particles. Electrophoresis involves the movement of a charged particle in a spatially uniform dc electric field. Other promising techniques involve spatially nonuniform ac electric fields. One of them is conventional dielectrophoresis which involves the movement of a noncharged but polarizable particle in a spatially nonuniform ac electric field. The other is travelling wave dielectrophoresis which involves the translation of a particle by a travelling electric wave that is generated by the spatial variation of phase of an applied voltage. Compared to other available methods, ac dielectrophoresis is particularly well-suited for the manipulation of minute particles in microfluidics (Koch et al., 2000, Gascoyne et al., 2002) because the application of an ac field suppresses undesirable electrolytic effects and electro-convection in the liquid, and employs polarization forces that are insensitive to the particle charge which is difficult to control. The use of ac electric fields can aid in the trapping of DNA, separation of cancerous and noncancerous cells, detection of biological warfare agents such as anthrax and smallpox spores, as well as the detection of toxic volatile airborne BTEX (benzene,m-toluene, ethybenzene and xylenes) (Heller, 2003, Gascoyne et al.,1992).

Micro-total-analytical systems (μTAS s) for analyzing chemical/biological substances are now used across a wide variety of domains ranging from biological warfare agent detection to the healthcare industry (Meldrum et al., 2002, Stone et al., 2001, Koch et al., 2000, Gascoyne et al., 2002, Pohl, 1978). The first step in the operation of a μTAS consists of concentrating and separating the analytes of interest from the background matrix and positioning them into selected locations for subsequent analysis. Dielectrophoresis has a promising potential for such applications. The heart of dielectrophoretic devices is a channel equipped with an array of electrodes capable of generating a high-gradient ac field that drives an analyte to the regions of high field strength (*positive* dielectrophoresis) or low field strength (*negative* dielectrophoresis), depending on whether it is more or less polarizable than the suspending liquid (Gascoyne et al., 2002). However, to date very little has been achieved towards understanding the micro-scale behavior of a suspension subject to a high-gradient electric field and shear in that the concepts currently favored for the design and operation of dielectrophoretic micro-devices adopt the approach used for macro-scale electric filters (Pohl 1978, Chang et al.,1995). A sound physical understanding of micro-scale dielectrophoretic phenomena is critical for their use in microfluidic devices (Ouellette, 2002).

1.2 Scientific and Technical Objectives

The main purpose of this study is to address micro-scale phenomena in a suspension subject to shear and a high-gradient strong ac electric field. A novel type of microfluidics which is equipped with dielectrophoretic gates was designed and fabricated using Sandia National Laboratories Surface Micromachining with Integrated Fluid Technologies (SwIFT^{TM}) process. Sandia's technology employs a sophisticated multilayer process which enables the development of complex fluidic, mechanical, and electrical microstructures. Using dielectrophoretic micro-devices, experiments were conducted on suspensions over a broad range of flow and electric field parameters to investigate how these characteristics affect the concentration and separation of particles. Experimental data were compared with theoretical predictions. The theoretical hypothesis was proposed that particles could be separated and concentrated in a suspension as a result of field-induced phase transition. Furthermore, biological and non-biological particles could be separated from one another.

CHAPTER 2

DIELECTROPHORESIS

2.1 Definition

Dielectrophoresis, a term introduced by H.A. Pohl in 1951 (Pohl, 1978, Jones, 1995), is the movement of a neutral but polarizable particle in a nonuniform electric field. Pohl performed early experiments with small plastic particles suspended in liquids and found that the particles would move upon the application of a nonuniform ac or dc field. The Greek term “phoresis” means force, and combining this with the term dielectric produces an expression which describes the force exerted on a dielectric particle due to the particle polarizability (Jones, 1995).

2.2 Interaction of a Particle with an Electric Field

Dielectrophoretic phenomena in a suspension typically encompass two fundamentally related but different types of electric forces. These include the forces exerted on individual particles by a spatially nonuniform external electric field referred to as the dielectrophoretic (DEP) force and the forces due to the electric interactions between the suspended particles caused by their polarization. The interparticle interactions include the mutual field-induced attractive or repulsive forces between two or more closely spaced particles.

The following characteristics describe the dielectrophoretic motion of a single particle caused by an electric field. In general, a particle experiences the DEP force only in a spatially nonuniform electric field. The DEP force is observed with both ac and dc excitation. If at a specified frequency the permittivity of a particle is greater than the permittivity of the surrounding medium, it is attracted to regions of a strong electric field. This is known as positive dielectrophoresis. Conversely, when the permittivity of a particle is less than that of the surrounding medium, the particle will experience negative dielectrophoresis and move towards the low field region. The DEP force is most easily observed in particles with diameters ranging from about 1 $\mu\mathrm{m}$ to about 1 mm (Jones,1995).

The induced dipole moment of a sphere of permittivity ε_p^* immersed into a fluid of permittivity ε_f^* is given by (Jones, 1995):

$$\vec{\mu} = 4\pi a^3 \varepsilon_0 \varepsilon_f \left(\frac{\varepsilon_p^* - \varepsilon_f^*}{\varepsilon_p^* + 2\varepsilon_f^*}\right)\vec{E} \tag{2.1}$$

where a is the particle radius, $\varepsilon_0 = 8.854\,10^{-12}\,\mathrm{F/m}$ is the vacuum permittivity, $\beta(\omega) = \frac{\varepsilon_p^* - \varepsilon_f^*}{\varepsilon_p^* + 2\varepsilon_f^*} = \frac{\varepsilon - 1}{\varepsilon + 2}$ with $\varepsilon = \frac{\varepsilon_p^*}{\varepsilon_f^*}$ is often referred to as the Clausius-Mossotti factor or the polarizability per unit volume of the particle, and $\vec{E}$ is applied electric field.

Here the complex permittivity of material is defined as:

$$\varepsilon_x^* = \varepsilon_x - i\frac{\sigma_x}{\omega} \tag{2.2}$$

where

ε_x : dielectric constant;

σ : conductivity;

ω : angular frequency, $\omega = 2\pi f$, f is the frequency of ac field in Hz;

$i = \sqrt{-1}$.

The dielectrophoretic force exerted by a spatially nonuniform ac field on a polarized sphere immersed in a fluid is defined as (Jones, 1995):

$$F_p = \frac{3}{2} v_p \varepsilon_0 \varepsilon_f \operatorname{Re}[\beta(\omega)] \nabla E^2 \tag{2.3}$$

The force acting on a particle is proportional to the real component of the particle polarizability $\beta(\omega)$, This depends on the mismatch between the particle and fluid electrical properties and is proportional to the particle volume, v_p, and the gradient of the square of the electric field strength, ∇E^2.

If $\operatorname{Re}\beta(\omega)$ > 0, then positive dielectrophoresis occurs, and the particle will tend to move towards the high electric field region. Whereas if $\operatorname{Re}\beta(\omega)$ < 0 , negative dielectrophoresis occurs, and the particle will tend to move towards the low electric field region.

The sum of all forces acting on the particle is given by the following:

$$F_{total} = F_{deterministic} + F_{random} \tag{2.4}$$

The deterministic force is a combination of the gravitational, hydrodynamic, and dielectrophoretic forces; whereas, the random force is due to the Brownian motion. The following diagram (Figure 2.1) illustrates the main phenomena underlying technologies employing positive and negative dielectrophoresis of a particle.

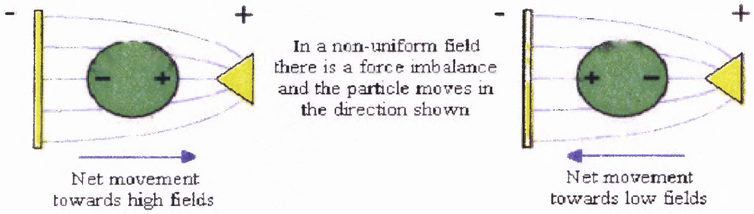

Figure 2.1 Positive and Negative Dielectrophoresis of a Polarized Particle. The left side shows relative particle polarizability greater than zero and the particle experiencing positive dielectrophoresis while the right side shows relative particle polarizability less than zero and the particle experiencing negative dielectrophoresis.

Another technique, which employs an electric field to generate the motion of particles immersed into a fluid is referred to as electrophoresis (Jones, 1995). In comparison with dielectrophoresis, electrophoresis is the motion of a charged particle through a spatially uniform electric field. A negatively charged particle will move towards a positive electrode while a positively charged particle will move towards a negative electrode. Electrophoresis is related to the double layer formation at the surface of a particle. When particles are suspended in an aqueous medium, ions of one sign collect at the surface of the particle while a surrounding cloud of ions forms a protective surface charge from the bulk of the fluid. Upon the application of a dc field the charges become mobile. This creates a fluid flow parallel to the surface, and the particle moves as a result of shear stresses on the interface between the double layer and the fluid. Electrophoresis can also occur in an ac field but only at relatively low frequencies (Jones, 1995). The distortion of a double layer caused by an applied field produces the large dipole moment of a particle immersed into an aqueous solution (Figure 2.2).

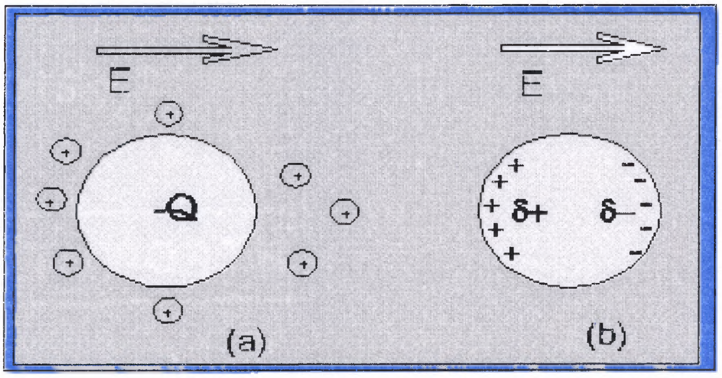

Figure 2.2 Electrical Dipole Moment (a) Distortion of electrical double layer caused by an applied electric field E. (b) Interfacial charges induced at the particle boundary. These two effects produce large electrical dipole moments. http://www.ibmm.informatics.bangor.ac.uk/pages/science/basic.htm

There are several distinctions to be made between electrophoresis and dielectrophoresis. First, in dielectrophoresis the motion of the suspended particles is independent of the sign of the field and either ac or dc fields may be applied. In electrophoresis, the motion of the particle depends on the sign of the particle charge and the sign of the field. Changing the sign of the field results in the reversal of the direction of particle travel. Second, the dielectrophoretic force depends on the particle bulk properties and is proportional to its volume which scales as the cube of the particle radius. Electrophoresis is proportional to the particle charge which is, in turn, proportional to the particle surface area which scales as the square of the particle radius. However, the particle charge also depends on the ionic strength of the fluid, and is thus more difficult to control than particle size. Third, dielectrophoresis requires spatially nonuniform electric fields whereas electrophoresis can be observed in either spatially uniform or nonuniform fields.

Fourth, dielectrophoresis is typically used with high field strengths; whereas, electrophoresis is usually used with low fields. Moreover, dielectrophoresis requires a substantial difference in the permittivity of the fluid and that of the particle. Electrophoresis can be observed even when the free charge per unit mass of the particle is small.

Finally, dielectrophoresis is most easily observed using relatively large particles in gases or liquids of low viscosity. Although the fields are high, they should be controlled so as not to cause overheating or space-charge effects. Dielectrophoresis can often be overwhelmed by side effects such as convection, turbulence, or even electrophoresis (Pohl, 1978).

2.3 Interparticle Electric Interactions

When an electric field is applied to a suspension, each particle acquires a dipole moment. If the field-induced interparticle dipole-dipole interactions are sufficiently strong the particles form into an organized structure of chains and columns which tend to align in the direction of the electric field (Figure 2.3). Since this phase transition results in a drastic change in the suspension rheology (from the fluid-like behavior to the solid-like behavior) it is often referred to as the electrorheological (ER) effect (Jones, 1995).

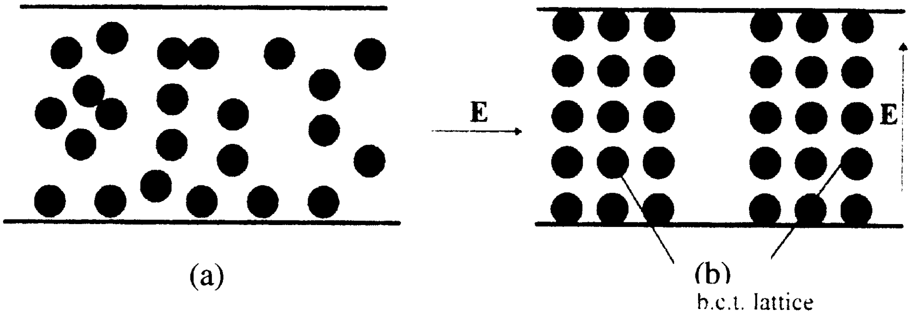

Figure 2.3 Field-induced Phase Transition in a Suspension. (a) The arrangement of particles before an electric field is applied. (b) The arrangement of particles following the application of a sufficiently strong electric field. The two parallel dark lines on the top and bottom show the electrodes.

The dipole-dipole interaction between two dielectric spheres of radius a (Figure 2.4) immersed into a dielectric fluid is (Jones, 1995):

$$F(d,\theta) = \frac{3}{16}\pi\varepsilon_o\varepsilon_p a^2\beta^2\left(\frac{a}{d}\right)^4[3\cos^2\theta - 1)\varepsilon_d + \sin(2\theta)\varepsilon_\theta]E^2 \tag{2.5}$$

where d is the distance between the two spheres and θ is the angle between the line connecting the particle centers and the electric field In this case ε_d and ε_θ are unit vectors in the radial and theta directions.

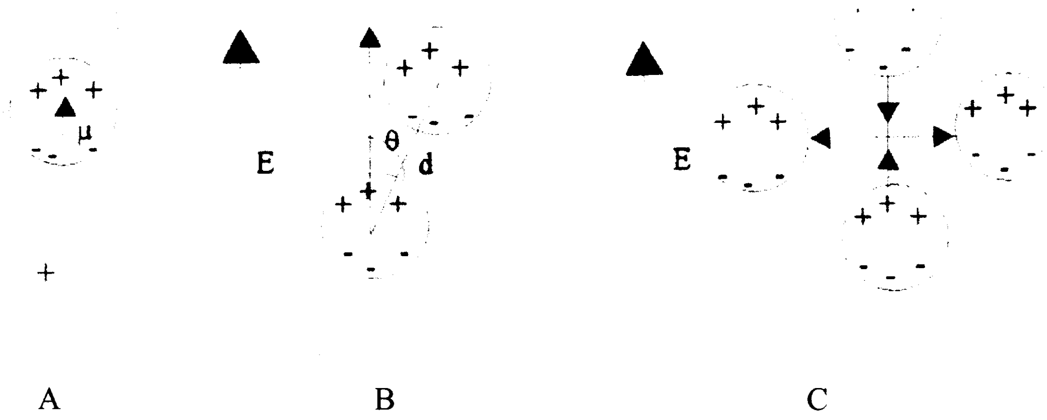

Figure 2.4 Polarization and Interaction Between Particles. (A) Particle polarization for $\varepsilon_p > \varepsilon_f$, (B) θ is the angle between the line joining the particle centers and the field direction, (C) the particles are attracted to each other when $\theta = 0$ and repelled from each other when $\theta = 90$ (Jones, 1995).

A theory for the field-induced phase transitions in low conducting suspensions caused by the interparticle interactions was developed by Khusid et al., 1995. This theory is based on the Maxwell-Wagner model of interfacial polarization of colloids (Dukhin et al., 1974, Russel et al., 1989) and the Lorentz model for describing long-range interactions of polarized particles (Landau et al., 1984). As part of the theory, the separation of a quiescent suspension into high and low concentration phases following the application of an ac field is described. One of the primary predictions of this theoretical model is that there is a similarity between the "concentration vs. temperature" phase diagrams for the phase separation in binary fluid mixtures with a high temperature miscibility gap and the "particle concentration vs. the field strength" of colloids subject to electric fields. This result provides a framework for understanding the morphology and kinetics of the aggregation patterns generated when an electric field is applied to a suspension. It also allows for the exploration of a large scope of experimental data and theoretical models available for the interpretation of the phase separation phenomena in binary systems (Markarian et al., 2002)

As a consequence of the theory, a complete set of phase diagrams has been developed. The phase diagrams are discussed in several publications (Khusid et al., 1996 and 1999, and Qiu et al., 2002). The diagrams are expressed in terms of λ and c where $\lambda = \frac{\varepsilon_o \varepsilon_f E^2 v_p}{k_B T}$ is the ratio between the electrical energy of the interparticle interactions and the thermal energy $k_B T$, and c is the volume fraction of the particles (Figure 2.5).

The random arrangement of the particles becomes unstable when the derivative of the particle chemical potential $\mu_p(c, \lambda)$ with respect to the particle concentration equals zero, $\partial \mu_p / \partial c = 0$, (Khusid et al., 1996 and 1999). The line $\partial \mu_p / \partial c = 0$ represents the spinodal curve in the phase diagram (Figure 2.5). The one-phase region of the phase diagram includes the random spatial arrangement of the particles, whereas the two-phase region corresponds to the appearance of a field-induced phase separation. On the coexistence curve, which separates the one- and two-phase regions, the values of the chemical potentials and of the osmotic pressures of the particles, $\Pi(c, \lambda)$, in the coexisting phases, c_1 and c_2, are respectively equal to each other (Khusid et al., 1996 and 1999).

$$\mu_p(c_1, \lambda) = \mu_p(c_2, \lambda) \text{ and } \Pi_p(c_1, \lambda) = \Pi_p(c_2, \lambda) \qquad (2.6)$$

The metastable and unstable domains are designated by M and U, respectively. These correspond to spinodal decomposition and nucleation, two mechanisms of the field-induced transitions in a suspension.

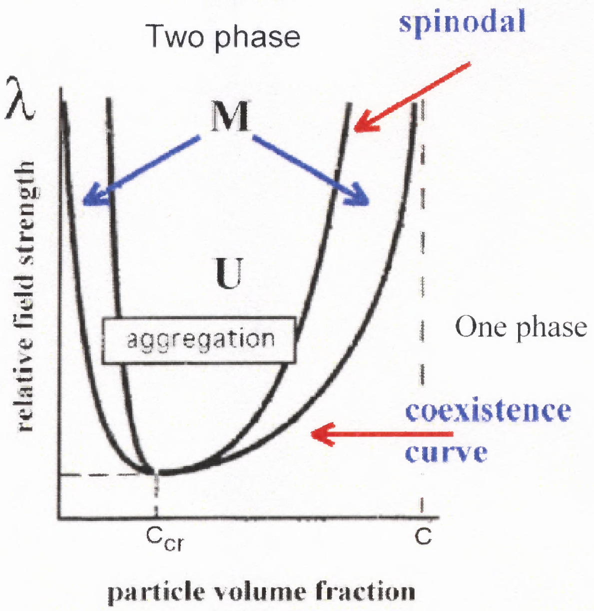

Figure 2.5 Phase diagram "the particle concentration vs. the field strength" of suspensions subject to electric fields: the metastable and unstable domains are denoted by *M* and *U*, respectively; λ is the relative strength of the field; and c is the particle volume concentration.

In (Qiu et al., 2002), the time scales for the behavior of a suspension under the application of an applied field are discussed. It is shown that the behavior of a suspension depends upon two time scales, τ_d and τ_a. The former represents the time required for a particle to move over the characteristic length of the system; whereas, the latter is the characteristic time for the field-induced structure formation in a suspension subjected to a spatially uniform field.

Under circumstances where there is a relatively rapid aggregation under conditions where the conductivity does not contribute to the interparticle interactions, and the applied field is strong enough to neglect Brownian motion the equation for τ_a given in (Shapiro et al., 1985, Has et al., 1993) can be applied (Khusid et al., 1999):

$$\tau_a \approx \frac{\eta_f}{\varepsilon_o \varepsilon_f (\mathrm{Re}(\beta)E)^2}\xi(\varphi) \quad , \quad \left[\xi \approx .4(\pi / 6\varphi)^{\frac{5}{3}} - 1\right], \ \mathrm{E} \sim \mathrm{V_{rms}} / \mathrm{d} \tag{2.7}$$

In this case, η_f is the viscosity of the suspending fluid, ξ is a coefficient that depends on the volume fraction of the particles, and $\mathrm{E} \sim \mathrm{V_{rms}} / \mathrm{d}$ is the field strength. The ratio $\left(\frac{1}{\varphi}\right)^{\frac{1}{3}}$ refers to the ratio between the average distance that two neighboring particles must travel in order to aggregate and the particle radius. When gravity forces and Brownian motion can be neglected the following ratio applies: $\frac{\tau_d}{\tau_a} = \frac{3d^2|\mathrm{Re}\,\beta|}{a^2\xi(\varphi)}$, where a is the particle radius and d is the characteristic scale of a dielectrophoretic device.

Khusid et al., 1996 found that under certain conditions dielectrophoresis would be accompanied by the field-induced phase separation. This would occur when a certain region of the suspension in which the pathway representing the local values of the particle concentration and the field strength in the suspension phase diagram would cross the coexistence curve on the phase diagram (Figure 2.5). In this case, it was found that the dielectrophoretic force would cause the particles to move into certain regions, and when their local concentration exceeds a critical value, to undergo a phase transition. These theoretical predictions were confirmed in experiments described in Chapter 6.

In this research, the author demonstrates that dielectrophoresis accompanied by the field-induced phase transition provides a powerful means for concentrating and separating biological and non-biological particles in continuously operating microfluidics.

CHAPTER 3

DESIGN AND FABRICATION OF MICROFLUIDICS

3.1 Introduction

There are many key processes involved in manufacturing of micro-electro-mechanical systems. Such steps include pattern replication, deposition, etching, sacrificial layer processing, and silicon planar technology. Every mass production technique requires automated methods of reproducing patterns. In the fabrication of ICs this is accomplished through photolithography (Habermehl 1998, Sniegowski et al., 2002)

Photolithography is a technique that involves the transfer of a pattern on a mask to a photosensitive material by means of ultraviolet light. In general, a series of aligned masks are used to fabricate complex structures. The masks are usually composed of a patterned thin film of chrome on quartz, and the pattern is usually transferred into photoresist on a silicon substrate. The photolithography process involves the application of photoresist and UV light. In addition, a mask is applied, and depending on the mask sensitivity to UV light negative or positive photolithography can occur. A thin film of a photosensitive material (the photoresist) is deposited on the substrate being processed. The film is then exposed through a plate (generally referred to as a 'mask') which contains an image of the pattern to be created. Depending on the resolution required the resist will be sensitive to visible light, ultra-violet light, X-rays or an electron beam. The photoresist is developed so as to expose the areas to be etched. The substrate is then exposed to an etching process which leaves behind the desired pattern in the substrate. Finally, the resist is removed to leave the patterned surface.

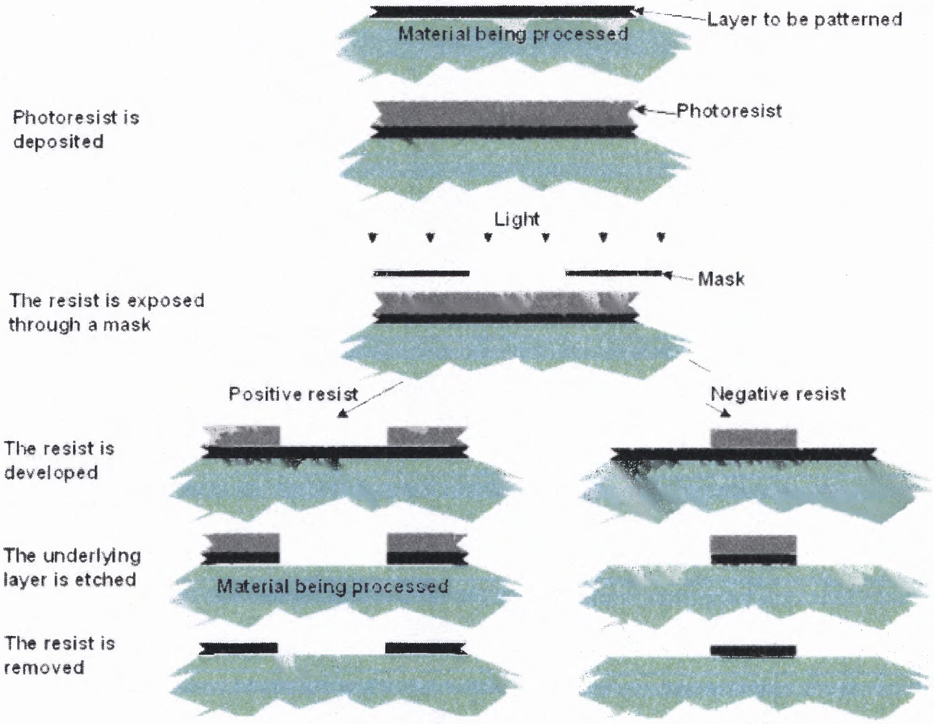

Figure 3.1 Photolithography. A thin film of a photosensitive material (the photoresist) is deposited on the substrate being processed. The film is then exposed through a plate (generally referred to as a 'mask') which contains an image of the pattern to be created.

http://www.ami.ac.uk/courseware/busben/restricted/ch5/busben05notes.html#5.3.1

The techniques used for deposition are epitaxy, vacuum deposition or sputtering, Chemical Vapor Deposition (CVD), spin coating, electroplating, and lift-off. The technique that is used in the fabrication of our devices is Chemical

Vapor Deposition (CVD). In this process a gas is passed across a heated sample in the reaction chamber, and a reaction takes place to produce the desired layer. This process is often used to create layers of silicon dioxide (SiO_2), silicon nitride (Si_3N_4), and polysilicon. A conformal coating results, and the added layer covers the entire surface.

3.2 Surface Micromachining

Surface micromachining involves the fabrication of micrometer-scale structures using the deposition and patterning of thin films on a base substrate, typically single-crystal silicon wafers. Photolithography is the technique used to transfer various patterns into bulk silicon substrates and thin films. Because surface micromachining is a batch fabrication process that uses conventional IC processing tools, high volume and low cost production may be achieved.

There are several basic steps in the surface micromachining process. Specifically, the construction of microelectromechanical structures requires particular steps to be taken in order to ensure proper device fabrication and function. In sacrificial layer processing, two or more materials are used and one is selectively etched away to leave a free-standing structure. SiO_2 is used as the sacrificial layer and polysilicon or silicon nitride is used for the structures. The selectivity ratio of the sacrifical oxide to nitride used in the SwIFT^{TM} process is 500:1. This means that sacrifical oxide will etch 500 times faster than nitride. One of the initial steps is to deposit or grow a dielectric layer on the bulk silicon substrate in order to provide electrical insulation between the thin film structures and substrate, as well as between different devices. The next step is to deposit and pattern a sacrificial layer onto the substrate. The third step involves the deposition and etching of polysilicon through a reactive etching process. Finally, wet release etching of the sacrificial layer can create a free-standing micromechanical structure.

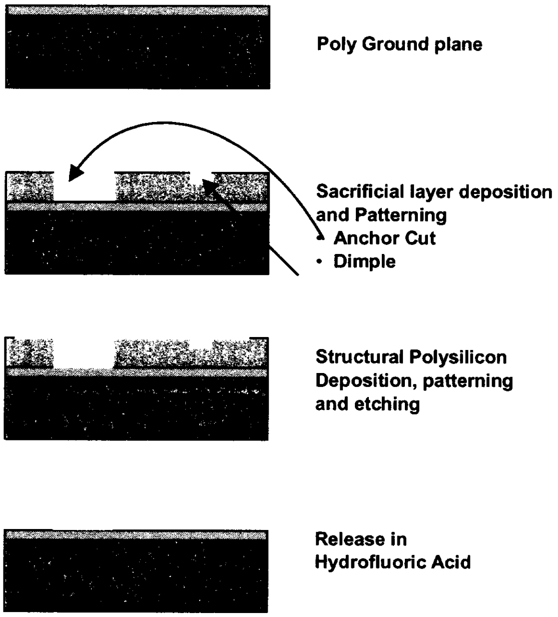

Figure 3.2 Steps in the surface micromachining fabrication process.

Microdevices specifically designed for use with fluids require further consideration in terms of fabrication. Typical microfluidic systems are constructed from plastics or glasses that are optically transparent and electrically insulating. This permits both optical interrogation of the system for analysis and detection, and allows the user to introduce localized electric fields into the system for fluid sample manipulation. An effective insulator is needed because microchannels of silicon, an electrical conductor, would short out electrodes that create electrical and magnetic fields used to analyze or manipulate the contents of the channel.

In order to avoid this problem channels were fabricated instead out of a version of silicon nitride. In the SwIFT^{TM} process, the construction is based on doped polysilicon; however, this causes a problem because doped polysilicon is a conductor, and in order to apply fields to the fluid, in particular biological fluids, an insulating structural material is needed. Manufacturing processes for silicon products strive for higher densities and small, sub-micron geometries, while bioMEMS and microfluidics often require thicker materials and larger features. Some other advantages of silicon nitride are that it is transparent, allowing researchers optical examination of the experiments, and that it is a material frequently used in microelectronic device fabrication (Galambos, 2001, Okandan et al., 2001a, Okandan et al., 2001b, MEMS short course, www.sandia.gov/micromachine).

Although the microdevices are fabricated step by step with lithographic processes well known to the semiconductor industry, the ability to make complicated devices is due to the Sandia SUMMiT V^{TM} fabrication process, which allows for five-level micromachine construction. The process uses 14 masks, which is about the same quantity as many CMOS IC processes (Galambos, 2001, Okandan et al., 2001a, Okandan et al., 2001b, MEMS short Course www.sandia.gov/micromachine).

3.3 The SUMMiT ™ and SwIFT ™ Processes

3.3.1 Introduction

Sandia National Laboratories uses a sophisticated version of AutoCAD to design parts in which each layer in the AutoCAD layout corresponds to a mask or process in the SwIFT ™ process. The drawings are designed and cross-sections can be viewed in order to examine connection points, spacings, and a thin film layer deposition. The modified multilayer SUMMiT V™ or SwIFT ™ process at Sandia National Laboratories was used to fabricate the microfluidics channels. The Ultra-planar multilayer process allows for the electrodes to be spaced very close together with a minimum distance of 1 µm. In addition, the modified SUMMiT V™ process allows for unique connections of the electrical leads to the bond pads. The multilayer surface micromachining allows for complex three dimensional structures in which conductive leads can be electrically isolated from each other laterally as well as vertically (see Appendix A). Finally, the multilayer SUMMiT V™ process enables complex systems and movable platforms with high force actuators to be manufactured. The layers involved in the standard SUMMiT™ and SwIFT ™ processes are described in Section 3.3.2.

3.3.2 Process Flow

The SUMMiT™ or SwIFT™ (Figures 3.3 and 3.4) process usually starts off with six inch bare wafer, (100) n type wafers, of 2 – 20 ohm-cm resistivity. Next, a 0.6 µm layer of thermally grown oxide silicon oxide (SiO_2) is deposited. A 0.8 µm layer of low-stress silicon nitride (SiN_x) is deposited on top of the oxide layer (Habermehl, 1998). Acting as an etch stop, the nitride layer protects the underlying oxide from wet etchants. These first two dielectric layers of low stress nitride and thermal oxide serve as electrical insulation between subsequent thin layers and the substrate.

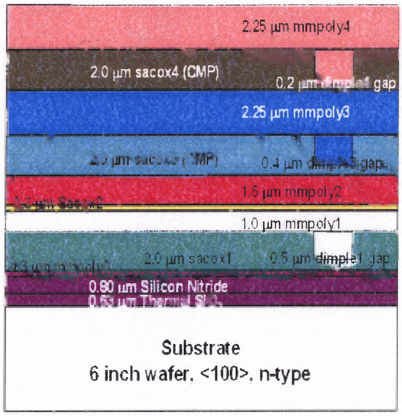

Figure 3.3 Standard SUMMiT^{TM} layers. Deposition of 4 layers of polysilicon without the silicon nitride layers.

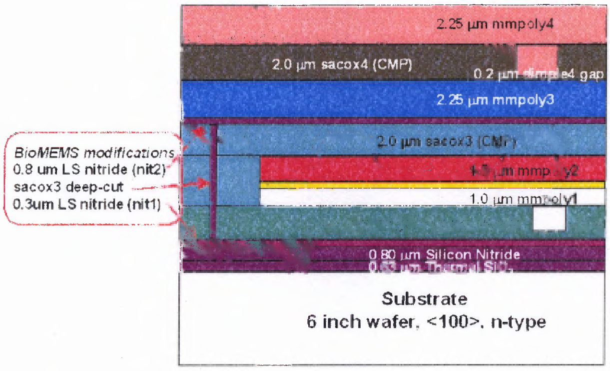

Figure 3.4 SwIFT^{TM} process. Modified flow for BioMEMS. The incorporation of the low stress silicon nitride layers allows for the creation of complex microfluidic structures and enclosed cavities with optical access and the ability to create almost any arbitrary field inside these structures.

The modified SUMMiT V^{TM} process includes layers of thermal silicon dioxide SiO_2, Silicon Nitride, Sacox1, Mmpoly0, Mmpoly1, Mmpoly2, Sacox3, Sacox2, Mmpoly3, Sacox4, and Mmpoly4. The layers Mmpoly0, Mmpoly1, Mmpoly2, Mmpoly3, and Mmpoly4 refer to micro-machined polysilicon layers while the Sacox layers refer to sacrificial oxide layers. The numbers 0,1, 2, 3, & 4 refer to the location of polysilicon in the modified Summit V^{TM} process with 0 being the first layer of polysilicon in the stack and 4 being the last layer of polysilicon. The Mmpoly0 layer is used for electrical interconnect and as a ground plane while the other poly layers are the mechanical construction layers. The polysilicon layers are composed of n-type fine grained polysilicon deposited from silane (SiH_4) in a low-pressure chemical vapor deposition furnace at approximately 580 $^{\circ}$C. The oxide films are typically deposited using LPCVD with the exception of the backfill oxide used prior to chemically mechanical polishing (CMP).

The thin film layers and masks used in the fabrication of the part are shown in Figure 3.5. The figure shows the masks used to form the channel with electrodes. In Figure 3.5 a, the set of masks used to form the bottom electrodes is shown. In Figure 3.5 b, the complete set of masks is shown. In Figure 3.5 c the channel with electrodes and sacrificial oxide is shown before the final release etch. The open channel after the final release etch is shown in Figure 3.5 d. The nitride cut mask is applied first and the backside Bosched-etched process is the final step. Bosch-etching is a process which consists of a $300\,\mu m$ diameter counter-bore backside partial etch into the Si substrate, followed by a $100\,\mu m$ diameter through-wafer etch to the channels on the front surface of the substrate. The Bosched-etched hole is shown in Figure 3.6.

www.oxfordplasma.de/process/sibo_1.htm

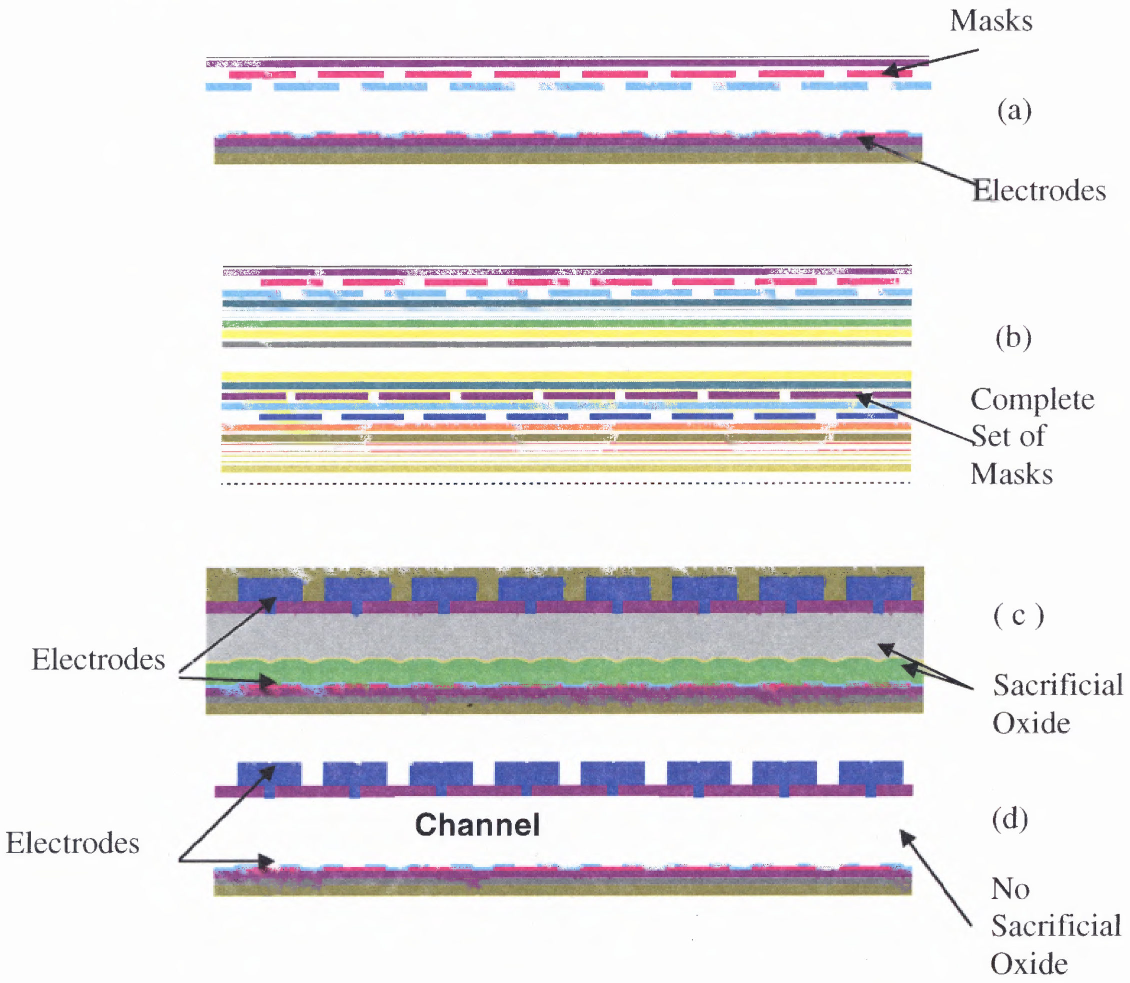

Figure 3.5 Masks Used in Fabrication of Microfluidic Channel. (a) Cross-section showing Nitride and Poly0 masks. Poly0 electrodes are formed (b) Masks and deposition layers used to make microfluidic channel with electrodes. (c) Cross-section of channel before release etch. (d) Cross-section of channel after final release etch.

The parts are typically released for 190 minutes in a ratio of 3:1 in REBC, Sandia developed (HF:HCL acid mixture). After acid bath etching, the parts are transferred to a round rinse tank containing DI water and 1 ml of tergitol. The parts are then rinsed for at least two hours allowing time for the HF to diffuse out of the long channels. Then, the parts are oxidized for 15 minutes. Parts are stored in methanol for one hour before drying in order to allow time for the methanol to diffuse in the channels. The parts are supercritically dried to prevent stiction.

3.4 Summary of Advantages of SUMMiT V^{TM} Multilayer Process and Surface Micromachining

The main reasons for being able to inexpensively manufacture these microfluidic channels are as follows. The process uses standard integrated circuit batch fabrication technology. The unique capabilities of the Sandia MEMS SUMMiT V^{TM} fabrication process allows for a sequence of deposition, patterning, and etching steps, and the use of silicon nitride to build insulated microchannels in that process. This process is repeated many times before resulting in the final device (Galambos et al., 2003, Okandan et al., 2001a, Okandan et al., 2001b, www.sandia.gov/micromachine).

3.5 Areas of Potential Problems and Improvement

One of the problems that occurs in the fabrication process is known as blowout. Sometimes during the final release process, the oxide layer becomes blown out connecting adjacent parts and creating multiple flow paths. The blowout occurs because the through-wafer bosch-etch keeps going outside the protected area, exposing the first dielectric layer oxide to the release etchant. The hydrofluoric acid, HF, sometimes eats away at the bottom oxide shown in Figure 3.6 causing and additional flow path in the channel. Although the oxide appears to be well protected by layers of Mmpoly0, Mmpoly1, and Mmpoly2, the HF somehow is still able to get to this lower oxide layer due to the Bosched-etched through hole being too large.

Trapped oxide is another problem. When the release etch time is not long enough the oxide can remain in the center of the channel. This will clog the channel and prevent fluid flow.

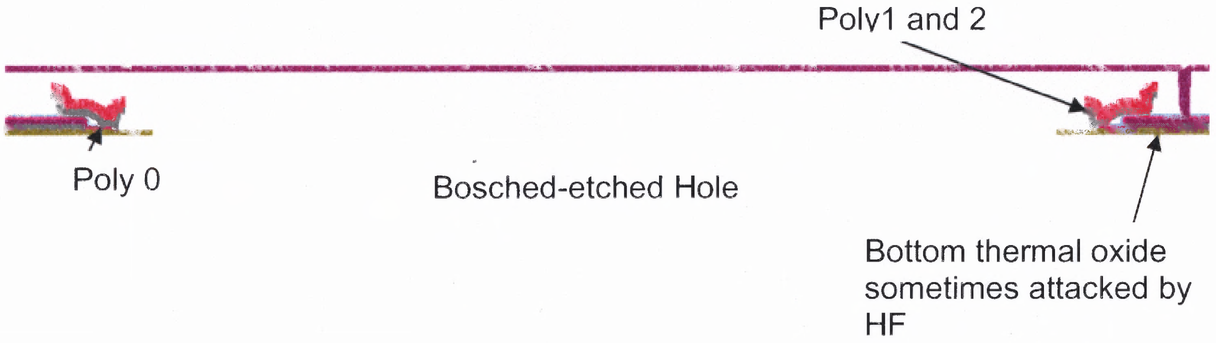

Figure 3.6 Cross-section through Bosched-etched hole. Part was designed using the layers Mmpoly0, 1, and 2. Mmpoly0 protects lower oxide from HF. The combined layer of Mmpoly1 and 2 potentially blocks the fluid flow. It is removed from later designs.

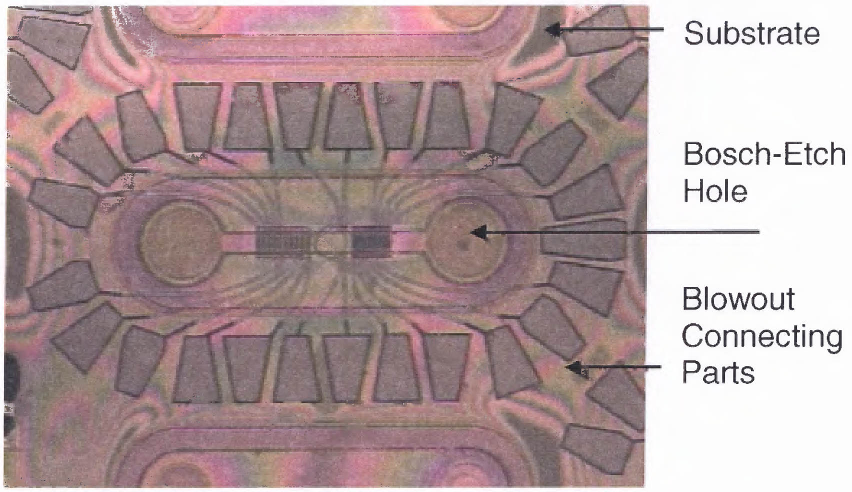

Figure 3.7 Microfluidic Channel with Blowout. Reticle Set 244 single part showing blowout. Reflection is due to nitride and substrate without the oxide.

In Figure 3.7 the region between the channels is blown out as shown by different colors being reflected. This can cause problems of liquid filling this region as well as shorting of electrodes. In Figure 3.8, however, there is very little blowout in the substrate region and around the part. Hence, Figure 3.8 shows a better part for testing.

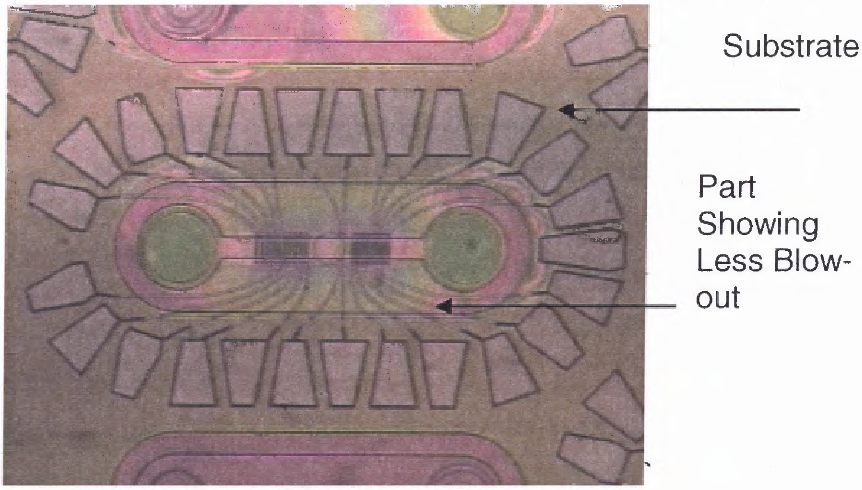

Figure 3.8 Microfluidic Channel Without Blowout. Reticle Set 244 microfluidic channel without blowout connecting adjacent parts. Part is not joined to other adjacent parts. Substrate is clearly shown.

Another potential problem in the fabrication process is that the seal between the electrodes and the nitride is not sufficiently tight. As shown in Figure 3.9 when this occurs the electrodes will short out and there will be no field generated.

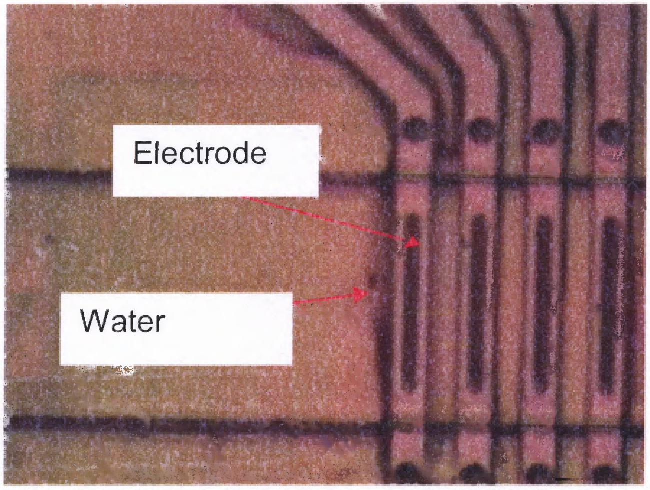

Figure 3.9 Electrode Shorting. Leakage around leads of electrodes which cause shorting. The seal between the nitride and the silicon is not tight.

The problem of the blowout may be eliminated by decreasing the size of the Bosch-etch hole. Increasing the length of the Poly 0 layer shown in Figure 3.6 may also help prevent etching of the thermal oxide and reducing blowout. Other problems such as trapped oxide may be corrected by increasing the release time of the part. The leakage problem could be corrected by coating the part with a thin layer of polydimethylsiloxane, PDMS.

CHAPTER 4

EXPERIMENTAL PROCEDURES AND RESULTS

4.1 Experimental Apparatus

The experimental set-up shown in Figures 4.1 and 4.2 consists of a microscope, a syringe pump, a function generator, a monitor, probes, as well as a CCD camera. It is assembled on a Probe Station in the Light lab at Sandia National Laboratories.

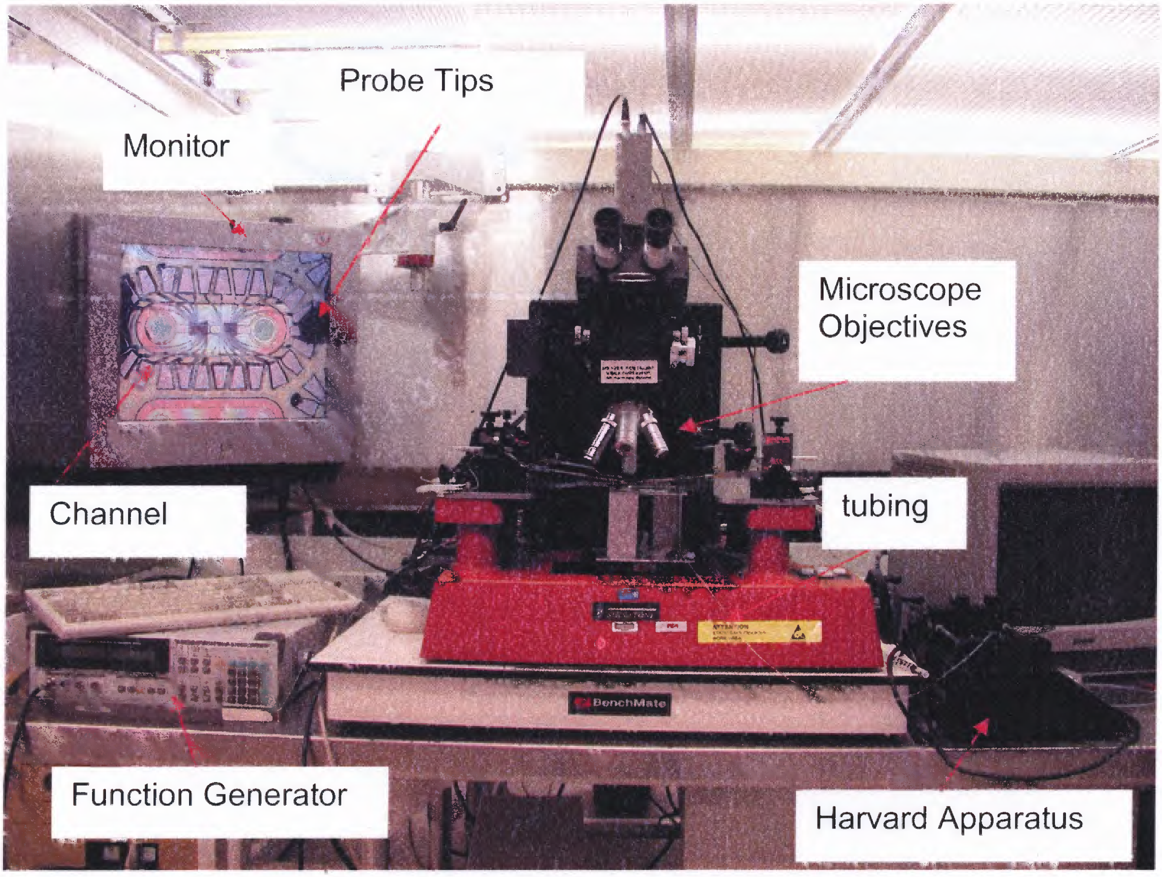

Figure 4.1 Experimental Set-up in the Light-Lab. Experimental apparatus includes a Harvard apparatus pump, a function generator, a microscope, probes, and a monitor, CCD Camera attached to microscope. Tubing is run from the syringe to the capillary.

The function generator is a Protek 9302 Synthesized Function/ Arbitrary Waveform Generator, Korea. This type of function generator allows for a maximum of 10 V peak to peak, 30 MHz. A Harvard PHD 22/2000 Advanced Syringe Pump NP 70-2001, Holliston, MA, is sometimes used to pump fluid through the syringe. In other cases the fluid is injected by manually pushing on the syringe. A Samsung SyncMaster Multifunction LCD 170 MP Monitor, Mexico, is used to view the image from the CCD camera mounted to the microscope.

Upchurch tubing is used to connect the syringe to the capillary in order to inject the fluid. A larger 1.0 mm OD and 0.01" ID tubing is attached to the syringe. Upchurch luer locks and fittings are used for attachments at both ends of this tubing. At one end, the tubing is attached to a syringe while at the other end the luer locks are used for attachment to a smaller 30 gage tubing. This narrower tubing, which attaches to the capillary, is a Double Hub Luer Lock tubing from Hamilton, 0.012" long, 0.030", OD and 0.012" ID. This 30 gage tubing is slid onto the capillary and securely sealed with Locktite Superglue gel.

The Probe Station is a Signatone Probing System, Santa Clara, California, Model S-250-6M, Serial #311. Probes are held in place by a vacuum and their position is adjusted longitudinally and laterally. The objectives allow for the channel view to be zoomed in and out. The place where the probes are being applied onto the silicon chip at the bond pad locations is indicated by the white circle on Figure 4.2.

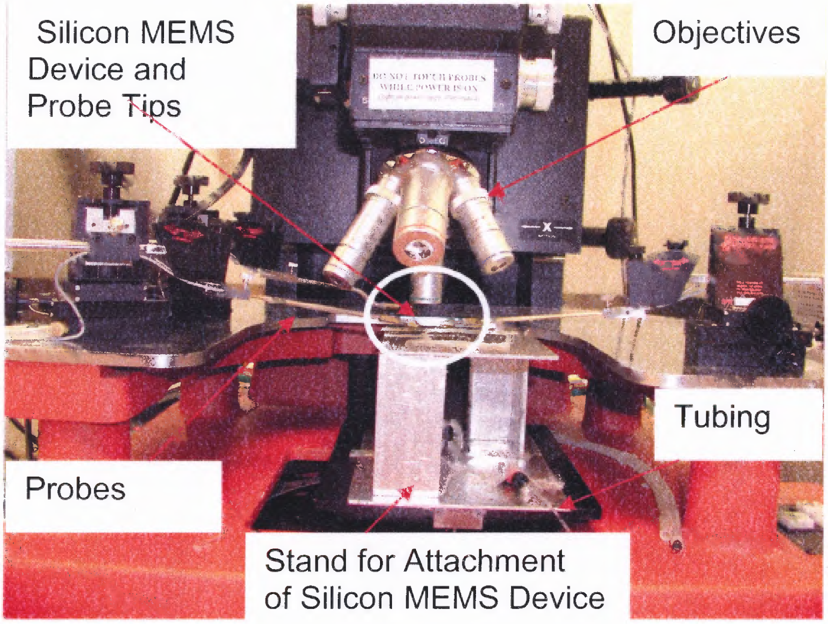

Figure 4.2 Close up View of Microscope and Objectives. Probes were used to apply the voltage to the bond pads. The objectives were 5x, 10x, 25x, and 50x. Tubing with suspension was from the syringe pump to the silicon MEMS device.

A silicon chip with several SwIFT^{TM} microfluidic designs is mounted onto a microscope slide. The slide is inverted for access to the Bosched-etched holes and steel capillaries are inserted into the channel, Figure 4.3. Glass or steel capillaries are glued to the access ports and then sealed with polydimethylsiloxane (PDMS, GE RTV615A) to prevent leaking. The PDMS is prepared by mixing together a curing agent and a rubber compound from GE Silicone Corporation. The ratio of the curing agent RTV 615B to the compound RTV 615A is 1:10. After mixing, the compound is placed around the capillaries and heated on a hot plate at 300 degrees Fahrenheit for 30 minutes. An acrylic based epoxy glue is sometimes used instead of PDMS to provide a tighter seal and to avoid clogging of the channel. Because the epoxy cured faster and is more viscous, it is typically found to work better than the PDMS especially with the larger Bosched-etched holes.

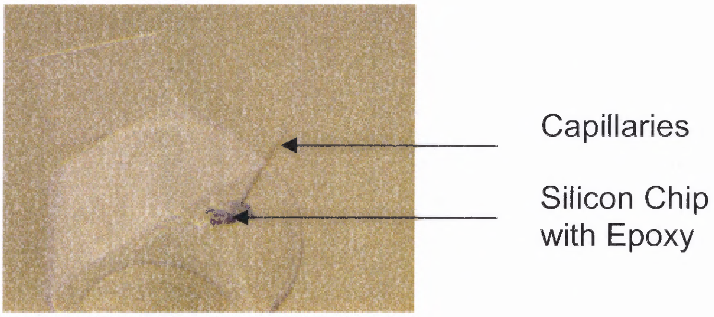

Figure 4.3 Silicon Device with Capillary Tubing. Silicon Chip is inverted and mounted onto a glass beaker. Steel or glass capillaries are placed into the backside Bosched-etched holes of the part and epoxy glue or superglue gel with PDMS is used to provide a leak proof seal.

After allowing the gel to dry for about 5 minutes, probes are then mounted onto the bond pads at the desired electrode locations as shown in the monitor in Figure 4.1. The electrodes are energized with a sinusoidal wave, 10V peak-to-peak and 15-30 MHz, using a function generator while the silicon substrate is grounded.

The Stereo Zoom 7 Microscope shown in Figure 4.4 is used to view the Bosch-etched holes and insert the capillaries. The silicon chip is inverted so that the Bosched-etched holes are viewed from the top. Afterwards, the capillaries are inserted and the sealant Locktite QuickTite Superglue Gel or epoxy is applied (Figure 4.5).

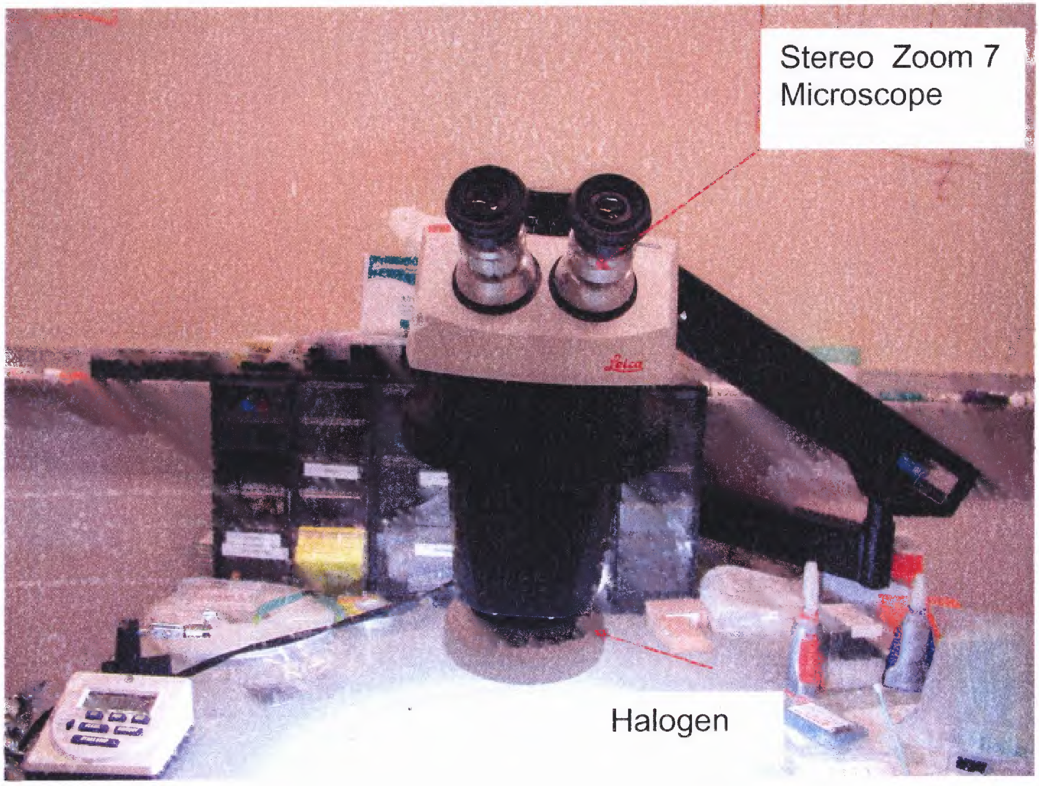

Figure 4.4 Microscope for installation of Capillaries. Stereo Zoom 7, Leica, Inc. Buffalo, NY, USA Model 312601, Rev A. Serial 11121 Microscope is used to view Bosched-etched holes for capillary installation.

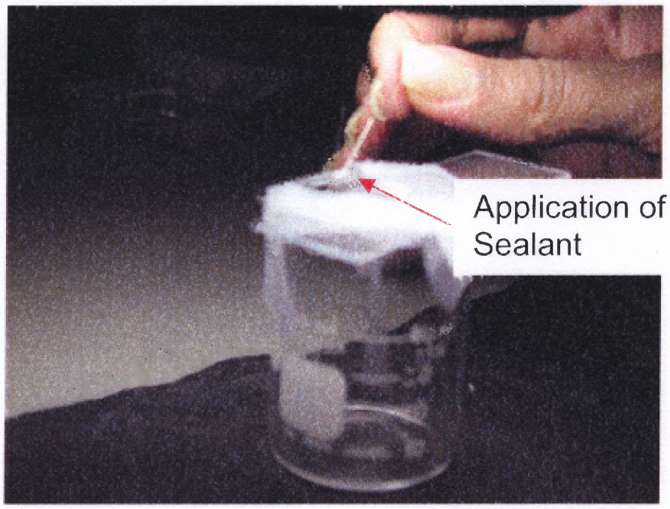

Figure 4.5 Manual application of PDMS, epoxy and glue to MEMS device.

The silicon MEMS device is glued to the slide. The slide is then inverted and taped to a glass beaker. A probe tip is typically used to apply the glue and PDMS around the capillaries.

4.2 Microfluidic Channel Design

A microfluidic channel with four layers of polysilicon and three nitride layers is shown in Figure 4.6. This part is used to study the effect of a nonuniform ac field on suspensions of polystyrene latex particles in DI water.

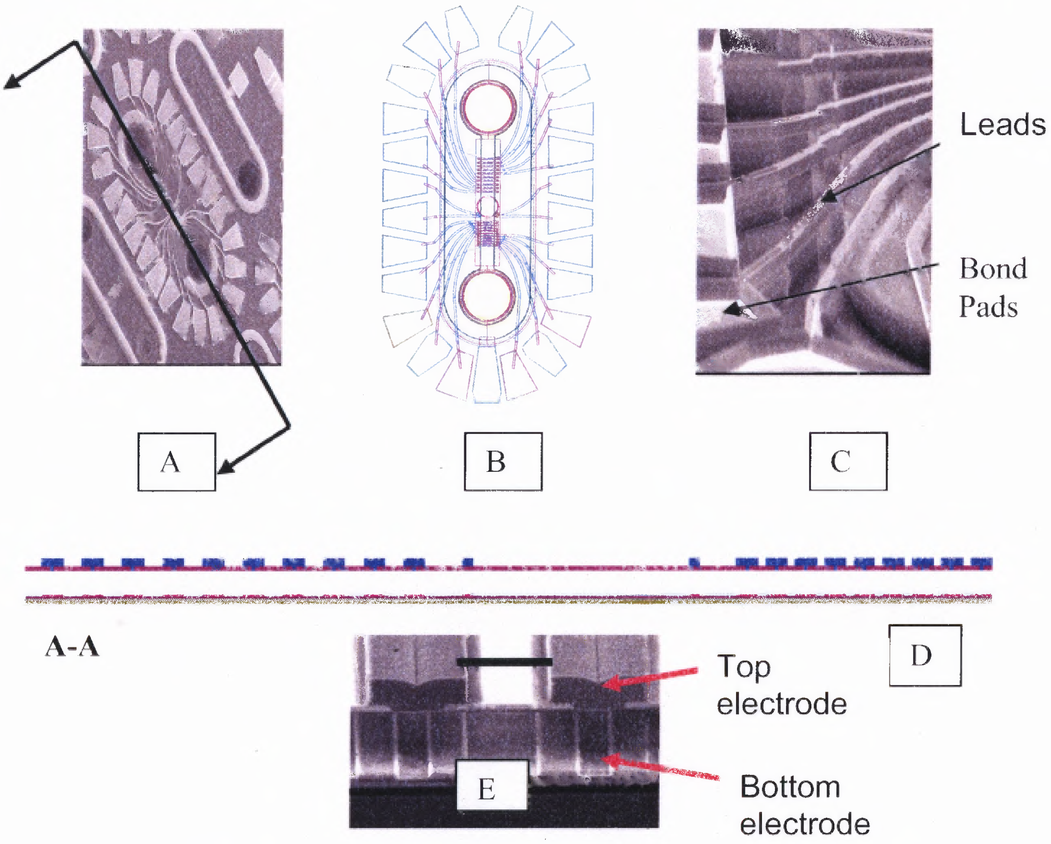

Figure 4.6 Microfluidic Channel Tested. (A) A flow channel with electrodes for creating/sensing electric and magnetic fields. (B) Autocad drawing of microfluidic channel showing layers for fabrication. (C) Close-up SEM image of polysilicon electrodes formed around the silicon nitride channel structure. (D) Cross-section of microfluidic channels showing exposed electrodes. Polysilicon electrodes are 6 μm wide with a 1μm nitride cut on the top and a 2 μm nitride cut on the bottom electrodes. The spacing between the polysilicon layers is 5 μm on one side and 2μm on the other side. The height of the channel is 6 μm. (E) Focused Ion Beam (FIB) image of cross-section, Scale bar 5 μm.

CHAPTER 5

SIMULATION OF THE PARTICLE MOTION IN DILUTE SUSPENSIONS

5.1 Single Particle Model

The single-particle model for dielectrophoretic phenomena in a dilute suspension considers the forces acting on the particles and neglects the interparticle electric and hydrodynamic interactions (Qiu et al., 2002, Markarian et al., 2003). By balancing the dielectrophoretic force, the Stokes drag force, the gravitational force, and neglecting Brownian motion, the following equation is obtained for the local particle velocity $\mathbf{u}$:

$$6\pi\eta_f a[\mathbf{u} - \mathbf{v}_f(\mathbf{r})] = 2\pi\varepsilon_o\varepsilon_f a^3 \operatorname{Re}(\beta)\nabla E_{rms}^2(\mathbf{r}) + \frac{4}{3}\pi(\rho_p - \rho_f)a^3 g\mathbf{e} \tag{5.1}$$

η_f is the fluid viscosity

a is the particle radius

$\mathbf{u} - \mathbf{v}_f(\mathbf{r})$ is the particle velocity relative to local fluid velocity $\mathbf{v}_f(\mathbf{r})$

ρ_p and ρ_f are the particle and fluid densities, respectively

g is the gravitational acceleration directed along a unit vector $\mathbf{e}$

To compute the term ∇E_{rms}^2, Laplace's equation needs to be solved for the entire channel. The displacement of a particle $\mathbf{r}(t)$ which is initially located at $\mathbf{r}_o$ may be described by solving the equation:

$$\frac{d\mathbf{r}}{dt} = \mathbf{u}, \qquad \mathbf{r}\big|_{t=o} = \mathbf{r}_o \tag{5.2}$$

The single particle model can be used to quantitatively describe the particle motion in the one-phase region of the suspension phase diagram "the particle concentration vs. the field strength" (Figure 2.5) and, furthermore, in the two-phase region of the phase diagram as long as the channel characteristics meet the requirement $\tau_d/\tau_a << 1$ referred to in Chapter 2 (Qiu et al., 2002, Markarian et al., 2003).

When the flow streamlines are arranged perpendicular to the xy plane of the electric field lines, components of the particle velocity in the x and y directions are not affected by the fluid flow. On the other hand, the particle velocity in the z direction (the flow direction) is not affected by the electric field, so that a particle will travel with the local fluid velocity in the z direction, which is described by the well-known expression for the parabolic fluid velocity profile along the cross-section of a parallel plate channel:

$$v_{fz} = 6U_a \frac{y}{H}\left(1 - \frac{y}{H}\right) \tag{5.3}$$

where $U_a = Q/A$ is the average fluid velocity with Q and A being the volumetric flow rate and the area of the channel cross-section and H is the channel gap. When the electric field lines are arranged in the yz plane the relative particle velocity, $\mathbf{u} - \mathbf{v}_f$, has components only in the y and z directions.

5.2 Simulation Results

The computer code for simulations of the field- and flow-driven particle motions based on the single-particle model was obtained from the Computational Fluid Dynamics Research Corporation (CFDRC), Huntsville, Alabama (http://www.cfdrc.com). The software is divided into three parts: CFD GEOM where the geometry and grid are created; CFD ACE where the problem is set up including the boundary conditions, initial conditions, and volume conditions; and CFD VIEW where the results are viewed, including the electric field configuration and the particle motions with animation. One starts off drawing the geometry in CFD GEOM. In GEOM the edges, faces, and grids are made. Once all the faces have been made, one can group the faces into a block and, if necessary, extrude into a 3D design. In addition, the inlets, outlets, walls, and type of medium are specified in CFD GEOM. Once the geometry has been completed, the next step is to apply the boundary conditions to the geometry in ACE. After applying the boundary conditions in ACE and setting up the problem, the simulation is run. Residual plots indicate whether or not the solution converges. The simulation results for the electric potential, the flow streamlines, and the particle trajectory can be observed using CFD VIEW. Animations of results can also be performed with CFD VIEW. Since the CFDRC code treats a particle as a point, it can be used to study the effects of the electric field configuration and shear flow on the particle motion when the channel dimensions are substantially greater than the particle size.

As an example, Figure 5.1 presents the computed distribution of the gradient of the square of the field strength, ∇E^2, for a channel equipped with electrodes on the top and the bottom. As can be seen from the Figure 5.1, ∇E^2 is more evenly distributed for the latter case when the electrodes are located on the top and bottom of the channel. A graph of the gradient of the electric field shows a more uniform distribution of the gradient for two levels of electrodes. The gradient is strongest at the electrode locations and weakest towards the center of the channel.

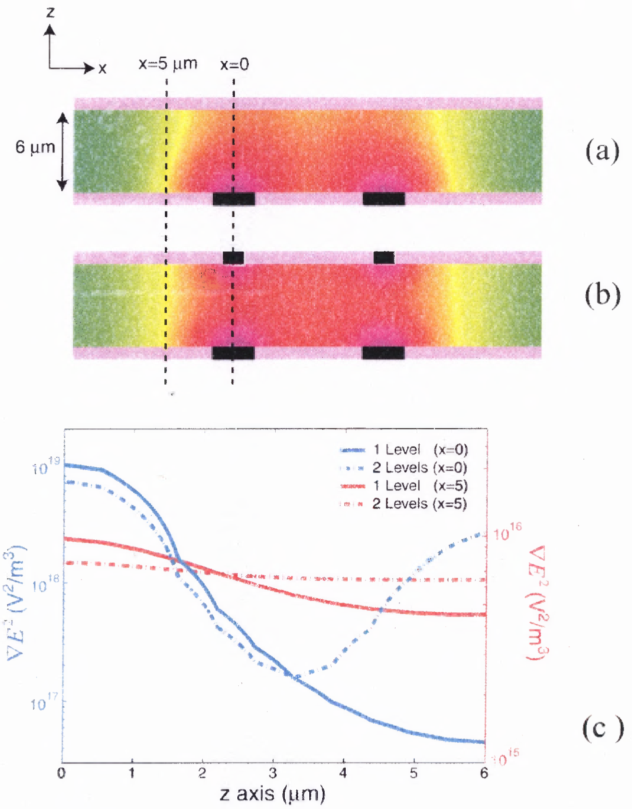

Figure 5.1 Gradient of Electric Field Squared. (a)The top figure shows the distribution of ∇E^2 when the electrodes are located only on the bottom of the channel. (b)The bottom figure shows the distribution of ∇E^2 when the electrodes are located on the top and bottom of the channel. (c) The bottom graph shows a plot of ∇E^2 as a function of channel height for both cases. (courtesy of C.D. James, Sandia National Laboratories).

The microdevices used in this study were equipped with electrodes arranged along the top and bottom of the channel. Experiments were conducted using suspensions of polystyrene latex beads and yeast and bacteria cells by applying 10 V peak to peak at 10-30 MHz. Over this frequency range, polystyrene latex beads exhibit negative dielectrophoresis, $\mathrm{Re}[\beta(\omega)] < 0$, whereas yeast and bacteria cells demonstrate positive dielectrophoresis, $\mathrm{Re}[\beta(\omega)] > 0$. Therefore, the beads are expected to accumulate away from the electrodes (in the light green region in Figure 5.1) while yeast and bacteria cells are expected to accumulate on the electrodes (the red region in Figure 5.1).

The results of 2D and 3D simulations of the motion of negatively and positively polarized particles under the action of a high-gradient electric field are presented in Figures 5.2 and 5.3, respectively. Initially, the particles are uniformly distributed throughout the channel (Figures 5.2a and 5.3a). Following the application of an electric field, the negatively polarized particles moved toward the low field strength region (the blue region in Figure 5.2b) whereas the positively polarized particles accumulated on the electrodes (Figure 5.3b).

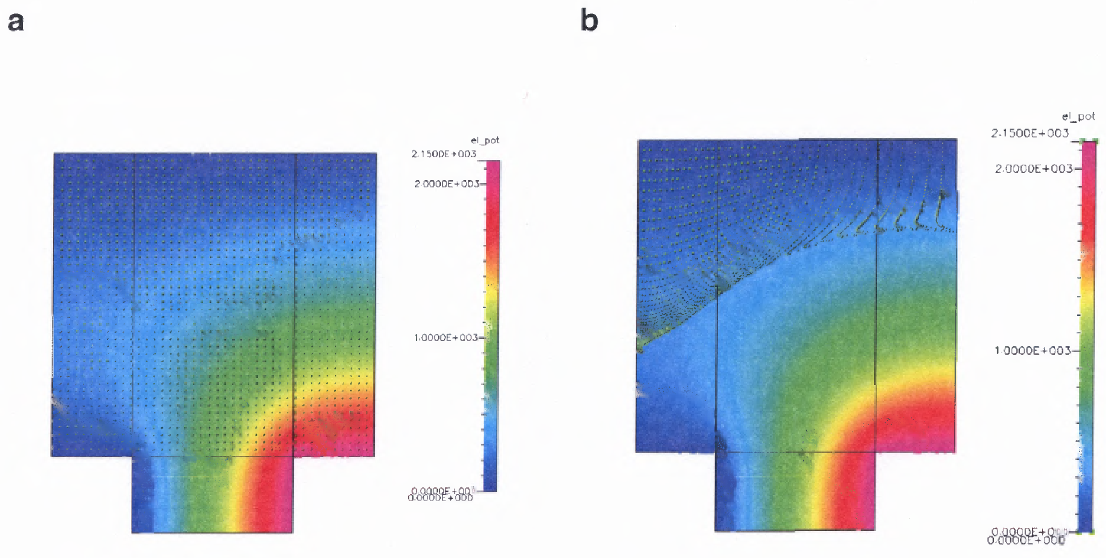

Figure 5.2 Negative dielectrophoresis, $\mathrm{Re}(\beta) < 0$. (a) Initial particle distribution. (b) The particle distribution following the application of an electric field for 10 s. Colors indicate the field strength.

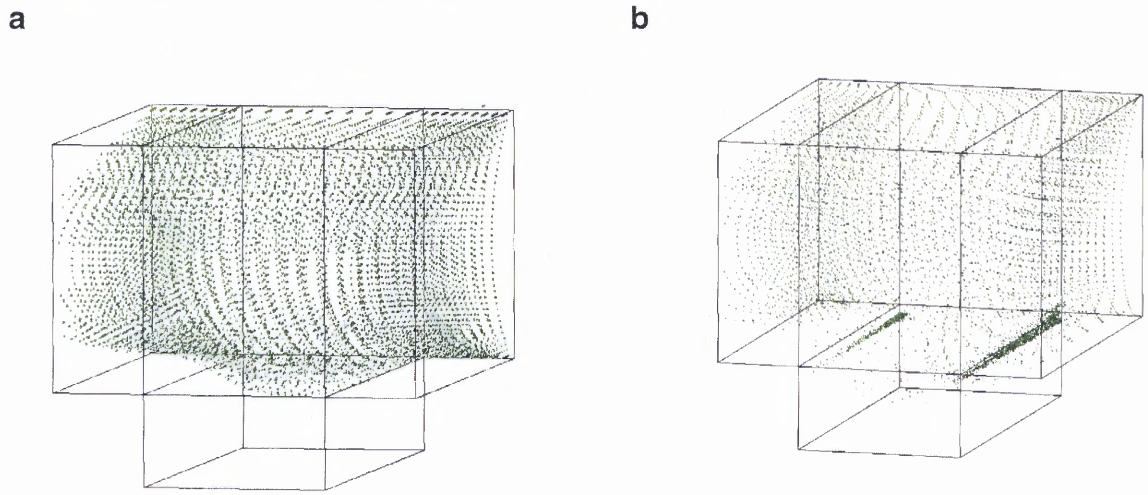

Figure 5.3 Positive dielectrophoresis, $\mathrm{Re}(\beta) > 0$. (a) Initial particle distribution. (b) The particles are collected on the electrodes following the application of an electric field for 0.02 seconds.

In addition to simulations of conventional dielectrophoresis, travelling wave dielectrophoresis was also modeled. Travelling-wave dielectrophoresis is the linear equivalent of electrorotation. However, instead of electrodes being arranged in a circle, they are laid out as "tracks", but the relationship of phases remains with each electrode. As a result, an electric field wave that "travels" along the electrodes is produced (Hughes et al., 1996). When a travelling wave interacts with a particle, it generates a dipole moment which follows the peak of electric field strength. If the travelling wave is moving sufficiently quickly, the dipole lags behind the field in a similar manner to that observed in electrorotation (Hughes, 1999, Jones, 1995). Because the wave is travelling in a linear instead of a rotational manner, a force rather than a torque is generated. Consequently, a particle will be moving along the electrodes like a train travelling along tracks, Figure 5.4 (Hughes, 1999).

Experiments were also run using travelling wave dielectrophoresis to separate white and red blood cells, as well as to separate a mixture of particles in a cross channel (Hughes et al., 1996, 1999). In both cases one set of particles will experience travelling wave DEP at a certain frequency whereas the other particles will not experience the travelling wave DEP force.

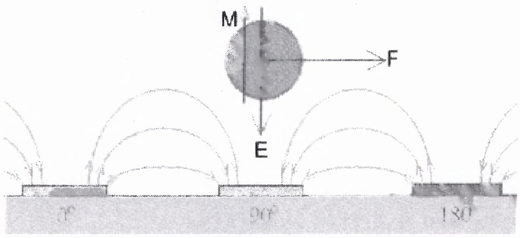

Figure 5.4 Travelling Wave Dielectrophoresis (Hughes et al., 1996, 1999).

Using permittivity values for erythrocytes and leukocytes found in the literature, as well as the conductivity of water, 0.001S/m, the real and imaginary components of the Clausius Mossotti factor, $\beta(\omega)$, were calculated and plotted with a short code from CFDRC, Figure 5.5. From the plots of the real and imaginary components of the Clausius Mossotti factor, the frequency value close to the intersection of these two curves was taken and tested in the CFDRC ACE solver. The translational motion of a particle in travelling wave dielectrophoresis occurs near the intersection of the two curves (Figure 5.6).

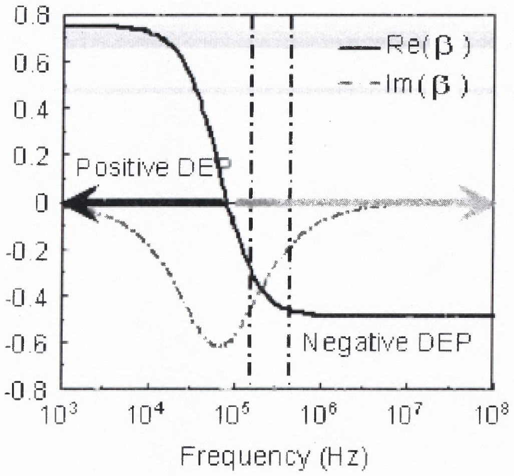

Figure 5.5 Typical Plot of Real and Imaginary Components of the Clausius Mossotti factor, β. The translational motion of the particle will occur at frequencies near the intersection of the two curves in the bracketed region.

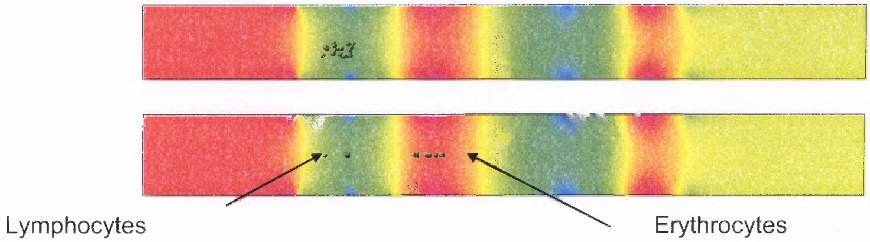

Figure 5.6 Distribution of the Electric Potential and the Location of Cells in a Microfluidics Channel. Positions of the particles in the beginning (the top figure) and following the application of a travelling electric wave (the bottom figure). Colors indicate the magnitude of the electric potential.

The same technique was used to simulate the particle motions in cross-channels (Figure 5.7). Results of simulations of the separation of a mixture of particles of permittivities 79 and 2.5 dispersed in water following the application of a travelling electric wave (applied voltage varies from +25 V to –25 V at 6.3 MHz) are shown in Figure 5.7. The mixture flows down the vertical channel and the particles having higher permittivity turn in the horizontal channel under the action of the travelling electric wave. The particles having lower permittivity continue moving with the flow along the vertical channel effectively separating the particles by type into two flow streams.

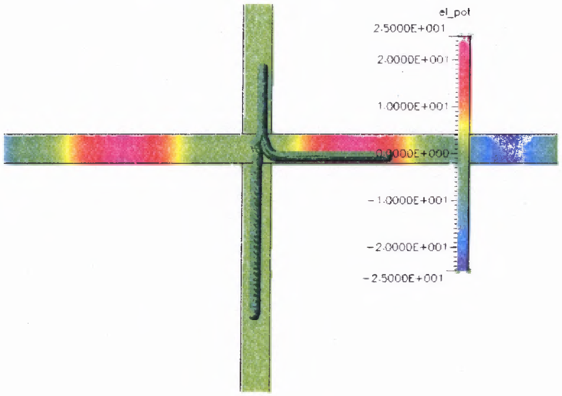

Figure 5.7 Cross-Channel Separation. Separation of a mixture of particles of permittivities 79 and 2.5 following the application of a travelling electric wave (+25 V and –25 V, at 6.3 MHz). Colors indicate the magnitude of the electric potential.

CHAPTER 6

FIELD-DRIVEN PHENOMENA IN A SUSPENSION FLOWING THROUGH A MICROFLUIDIC CHANNEL

6.1 Behavior of Dilute Suspensions

Flow experiments were conducted on 0.001% volume/volume suspensions of polystyrene latex beads in DI water. The intent of using such dilute suspensions was to study the particle motions over the frequency range from 1 Hz to 30 MHz when the interparticle dipolar interactions are negligibly small. In the case of a 30 MHz field, the particles were observed to be repelled from the high field region in the vicinity of the electrode (Figure 6.1). The repulsion force acting on the beads was found to increase with the frequency in the range from 100 KHz to 250 KHz (Figure 6.2). For 250 KHz, in particular, the particles were strongly repelled from the electrodes and approached the Bosched-etched hole whereas at 100 KHz the beads were located closer to the electrodes. The applied field was observed to pump the fluid for the field frequencies ranging from 1 Hz to 10 Hz. The amplitude of the electroosmotic flow generated at these frequencies for 10V is nearly twice as large as that for 5 V.

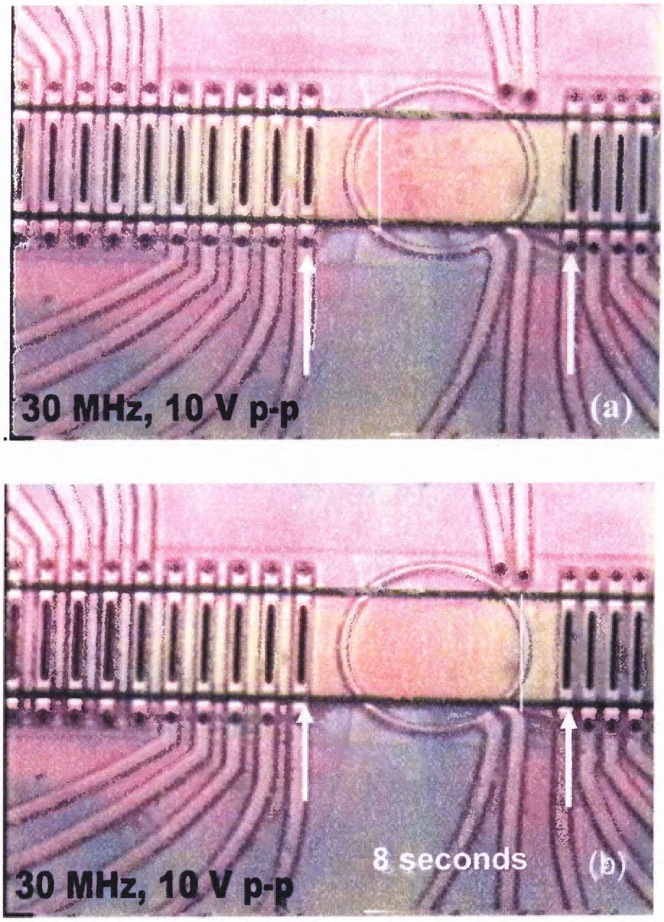

Figure 6.1 Negative Dielectrophoresis in a Dilute Suspension. A 0.001% suspension of polystyrene latex beads is placed in the microfluidics channel. After the exposure to the field for 8 seconds, 10 V p-p, 30 MHz, the beads move (a) from the center of the channel (b) towards the end of the channel. (Voltage applied at white arrow locations)

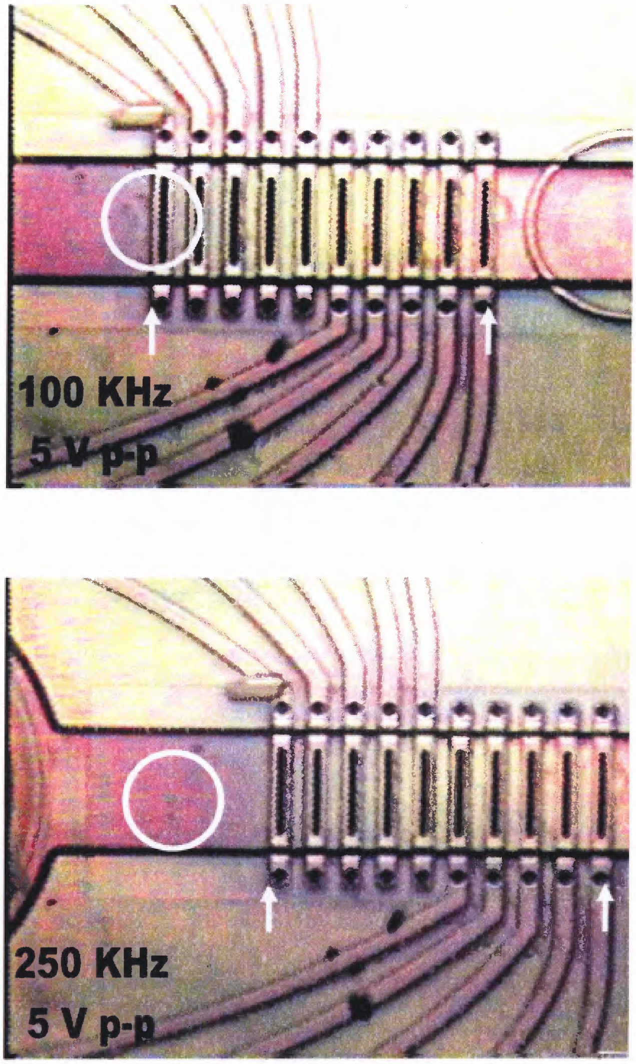

Figure 6.2 Effect of Low Frequency Electric Fields on a Dilute Suspension of Polystyrene Latex Beads. The bead location at (a) 100 KHz and (b) at 250 KHz (Voltage applied at white arrow locations).

6.2 Phase Transitions in Flowing Suspensions

To study the effects of the interparticle interactions on the suspension flow, experiments were performed on more concentrated suspensions of 0.1% v/v subject to high-frequency fields 10-30 MHz. Following the procedure proposed in

(Dussaud et al., 2000, Qiu et al., 2002), the value of the particle polarizability, $\beta(\omega)$, for this frequency range was calculated from the low-field (~ V/mm) measurements of the suspension complex dielectric permittivity, $\varepsilon_s^* = \varepsilon_s' - i\varepsilon_s''$, using the Maxwell-Wagner expression (Russel et al., 1989) for the concentration dependence of ε_s^* for randomly distributed spheres:

$$\left(\varepsilon_s^* - \varepsilon_f^*\right)/\left(\varepsilon_s^* + 2\varepsilon_f^*\right) = c\beta(\omega) \tag{6.1}$$

where ε_f^* is the complex dielectric permittivity of the DI water and c is the volume fraction of the spheres. The dielectric permittivities of the suspension and that of the DI water were measured using the standard technique of dielectric spectroscopy in a low electric field. The particle volume fractions, c, in suspensions used for these measurements varied from 0.1% to 10% (v/v). The measurements were performed with the use of a network analyzer, Agilent 8753. Plots of the imaginary and real components of β are shown in Figures 6.3(a) and (b). The bead polarizability was found to equal $\beta \cong -0.45 - 0.27i$ for 10-30 MHz. The negative value of $\mathrm{Re}(\beta)$ indicates negative dielectrophoresis.

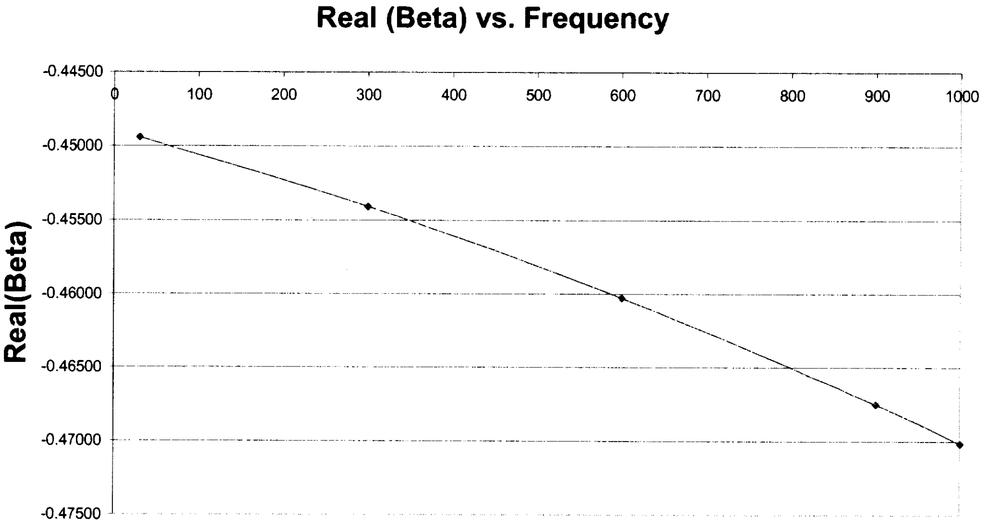

(a)

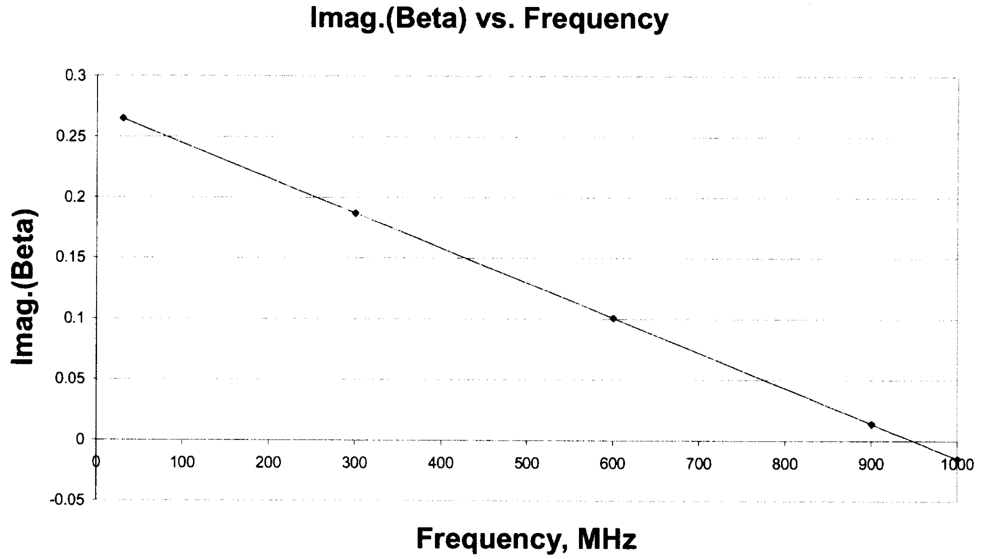

(b)

Figure 6.3 The Frequency Dependence of (a) Real and (b) Imaginary Components of the Particle Polarizability, β. (a) $\mathrm{Re}(\beta)$ gradually declines with increasing frequency. (b) $\mathrm{Im}(\beta)$ gradually decreases with frequency. The negative value of $\mathrm{Re}(\beta)$ indicates negative dielectrophoresis.

Experiments demonstrated that 0.1% v/v suspensions flowing through a micro-channel exhibited a new many-body phenomenon of dielectrophoresis accompanied by the field-induced phase separation which originates from the interparticle dipolar interactions (Bennett et al., 2003). The photos presented in Figure 6.4 show the time evolution of the particle distribution in a 0.1% (v/v) suspension from which it is evident that the beads, experiencing negative dielectrophoresis, are repelled from the dielectrophoretic gate and accumulate in a region near the electrodes (Bennett et al., 2003, Movie 1 deposit with EPAPS). On account of compressive electric and shear stresses, the layer of these beads formed a round bolus [Figure 6.4 (a)] with a distinct front between the regions enriched with and depleted of particles. As time progressed [Figure 6.4, (b)-(d)], the size of the bolus increased and its side close to the microelectrodes flattened. By taking the ratio of the volume of the beads entering the channel (cQt with Q and t being the flow rate and time, respectively) to the bolus volume, which was estimated, from the images (Figure 6.5) under the assumption that it spans the channel height, the average particle concentration in the bolus was found to run as high as 40-50% (v/v) in 180 seconds.

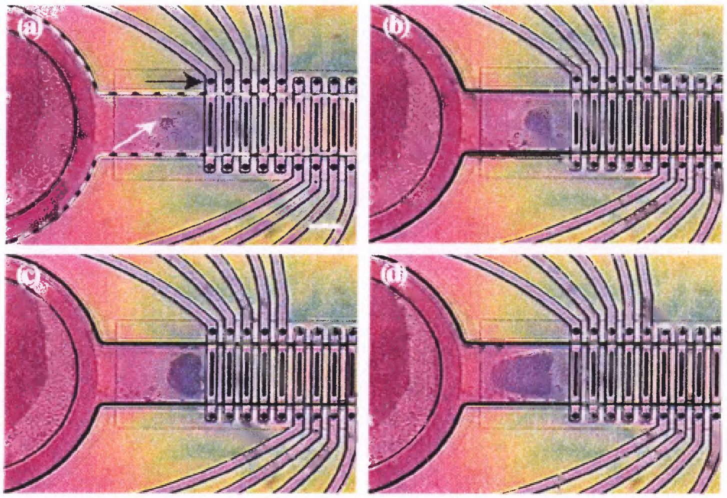

Figure 6.4 Bolus Formation Progression. Dielectrophoresis ($10\,\mathrm{V}$ p-p, 30 MHz) of beads accompanied by a phase separation (white arrow). The dashed lines denote the outline of the fluidic channel, and the black arrow indicates the energized electrode. The dark regions on the polysilicon traces indicate the places where the ceiling electrodes are in direct contact with the fluid. The time is (a) 10s, (b) 70s, (c) 120s, and (d) 180s. The flow was from left to right, with the flow rate ranging from 0.24 pL/s to 9.6 pL/s. Scale bar = $20\,\mu\mathrm{m}$.

Now consider an electro-hydrodynamic model which was proposed for simulating the bolus formation (Bennett et al. 2003). This model generalizes a thermodynamic theory (Khusid et al., 1995, 1999, and 1996) for the field-induced dielectrophoresis and phase separation of a suspension subject to an ac field (see Chapter 2). The proposed electro-hydrodynamic model encompasses the quasi-steady electrodynamic equations (Landau et al., 1984) with Equation (6.1) for ε_s^* together with the momentum and continuity balance equations of the "mixture" model for a suspension (Ungarish, 1993), which are averaged over the field oscillations. The suspension is viewed as an effective Newtonian fluid (Ungarish, 1993) with an effective viscosity $\eta_s = \eta_f \hat{\eta}(c)$ where η_f is the suspending fluid viscosity and $\hat{\eta} = [1 + 1.5c/(1 - c/c_m)]^2$ with $c_m \sim 0.63$ is the

Leighton-Acrivos expression (Ungarish, 1993). The bulk electric force, $\mathbf{F}_e$, exerted on a suspension, and the particle velocity relative to the suspending fluid, $\mathbf{v}_p$, are expressed in terms of the chemical potential of the particles (Khusid et al., 1995,1999) μ_p as:

$$\mathbf{F}_e = -c\nabla\mu_p, \qquad \mathbf{v}_p = \left[(1-c)^2 v_p / 6\pi a\eta_s\right]\left[-\nabla\mu_p + (\rho_p - \rho_f)\mathbf{g}\right], \tag{6.2}$$

$$\mu_p = (k_B T/v_p) f_0' - \varepsilon_0 \left[\partial \mathrm{Re}(\varepsilon_s^*)/\partial c\right]_{\omega t_c} \left\langle \mathbf{E}^2/2 \right\rangle \tag{6.3}$$

where ρ_p and ρ_f are the densities of the particles and of the fluid, $\mathbf{g}$ is the gravitational acceleration, the first term in Equation (6.3) refers to the chemical potential of the particles in the absence of the electric field (Russel et al., 1989), $k_B T$ is the thermal energy, t_c is the dielectric relaxation time (Khusid et al., 1995), and $\langle \; \rangle$ denotes time averaging over the field oscillation. In particular, Equation (6.3) predicts the phase diagram "the particle concentration vs. the field strength" (Figure 2.5) of a suspension subject to a spatially uniform ac electric field. In the framework of the proposed model, the interparticle electric and hydrodynamic interactions are incorporated through the concentration dependence of μ_p, η_s, and the hindrance factor $(1-c)^2$ in Equation (6.2). It is important to point out that the electro-hydrodynamic model, Equations (6.1)-(6.3), contains no fitting parameters provided that $\beta(\omega)$ is measured in low fields (Figures 6.3). For $c \to 0$, Equations (6.1)-(6.3) lead to the single-particle model (Chapter 5) which is consistent (Dussaud et al. 2000, Qiu et al. 2002, Markarian et al. 2003) with experimental data for dilute suspensions.

Depicted in Figure 6.5 is the simulation of the time evolution of the particle distribution using the data for water, for the particle properties, and for the channel dimensions presented above (Bennett et al., 2003, Movie 2 deposit with EPAPS). As can be seen, the particles, which accumulate in the region close to the microelectrodes, undergo a field-induced phase separation and form two concentrated layers near the channel top and bottom [Figure 6.5(a)]. As time progresses, these layers increase in size and eventually span the channel gap forming a bolus whose side adjacent to the electrodes flattens [Figure 6.5 (b, c)]. As the bolus grows, the opening of the channel cross-section decreases causing the flow velocities [Figure 6.5 (a) to (c)] and the particle velocities [Figure 6.5 (e) to (g)] to increase with time. The direction of the particle velocities indicates that particles primarily join the bolus at the side closest to the electrodes. The theoretical predictions for the bolus growth, for the particle concentration in the bolus, and the fact that particles travel around the circumference of the bolus and are then drawn into the bolus side closest to the electrode, are consistent with the observations (Figure 6.4). In line with the experiments, the simulations indicated that experimental conditions lie in the transition region between the formation of one bolus located near the channel centerline and two boluses attached to the channel side walls. For example, a slight change (~8%) in the voltage distribution along the microelectrode leads to the appearance of two boluses [Figure 6.5(d,h)].

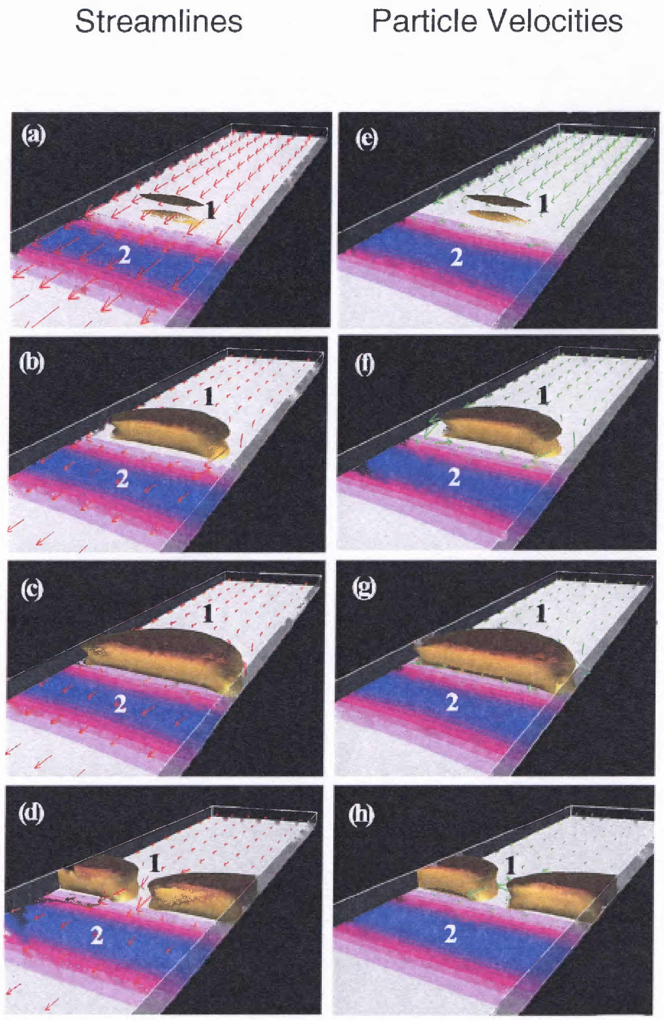

Streamlines

Particle Velocities

Figure 6.5 Numerical simulations of the concentration contours. (1) for the $0.1\%(\mathrm{v/v})$-suspension, 8.64 pL/s, $10\,\mathrm{V}$ p-p. In the panels, the fluid flow is from the upper right-hand corner to the lower left-hand corner. The color band (2) indicates the variation of E^2 along the channel bottom (white for up to $1.3kV^2/cm^2$, pink for $1.3-2.7kV^2/cm^2$, and blue for $10.6-11.9kV^2/cm^2$), whose maximum is located near the first electrode (Figure 6.4). Time is (a, e) 10s, (b, f) 70s, (c, g) 180s, and (d, h) 120s. The computed values for $\mathrm{c}_{\max}$ in the bolus [in $\%(\mathrm{v/v})$] are (a) 8.73, (b) 45.4, and (c) 56.4, and (d) 54.1. In (a) to (d), the red arrows show the relative magnitude of the flow velocity [$\mathrm{v}_{\max}\big|_{t=0} = 36\mu\mathrm{m/s}$; $\mathrm{v}_{\max} =$ (a) $49.8\mu m/s$, (b) $106.3\mu m/s$, (c) $110.4\mu m/s$, and (d) $139.9\mu m/s$]. In (e) to (h), the green arrows show the relative magnitude of the particle velocity, $v_{p,\max}\big|_{t=0} = 36\mu m/s$, $\mathrm{v}_{\mathrm{p,max}} =$ (e) $45.2\mu m/s$, (f) $78.8\mu m/s$, (g) $151.4\mu m/s$, and (h) $171.6\mu m/s$].

The photo in Figure 6.6 illustrates the dielectrophoretic separation of a heterogeneous mixture of polystyrene beads and heat-killed bacterial cells (Staphylococcus aureus; Molecular Probes) dispersed in DI water. The beads, experiencing negative dielectrophoresis, form two boluses adjacent to the channel walls [similar to the simulation results shown in Figure 6.5 (d, h)]; whereas the cells, which are more polarizable than DI water at this frequency, experience positive dielectrophoresis and are collected on the electrode. The complete separation of the continuously flowing cell-bead mixture was achieved by cycling the activation of the electrode on and off (Bennett et al., 2003, Movie 3 deposit with EPAPS). During the off phase, the cells and particles which were dielectrophoretically separated during the on phase, maintained their spatial separation and were carried along the channel to the outlet port, but, before the beads had reached the edge of the leading electrode, the field was turned back on, thereby repelling the beads again (Figure 6.6) to a distance $\sim 20\,\mu\mathrm{m}$ from the electrode edge. In contrast, the cells which had not been collected on the electrode continued moving with the flow towards the outlet port of the device.

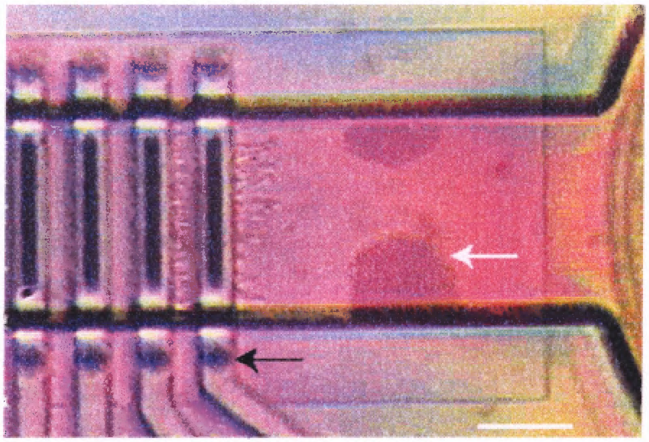

Figure 6.6. Particle and Cell Separation. Dielectrophoretic (10V p-p, 15 MHz) separation of bacterial cells and beads. The cells adhere to the energized electrode (black arrow) while the beads experience negative dielectrophoresis accompanied by a phase separation (white arrow). The flow is from right to left, with the flow rate ranging from 0.24 pL/s to 9.6 pL/s. Scale bar = $20\,\mu\text{m}$.

The location of the bolus as a function of frequency and voltage was also studied. It was found that increasing the voltage increased the negative DEP repulsion force on the beads and pushed the bolus back a greater distance along the channel (Figure 6.7). The bolus location varied uniformly with voltage and thus the location can be determined graphically. However, the variation of bolus location with frequency was also studied but was not found to be extremely uniform.

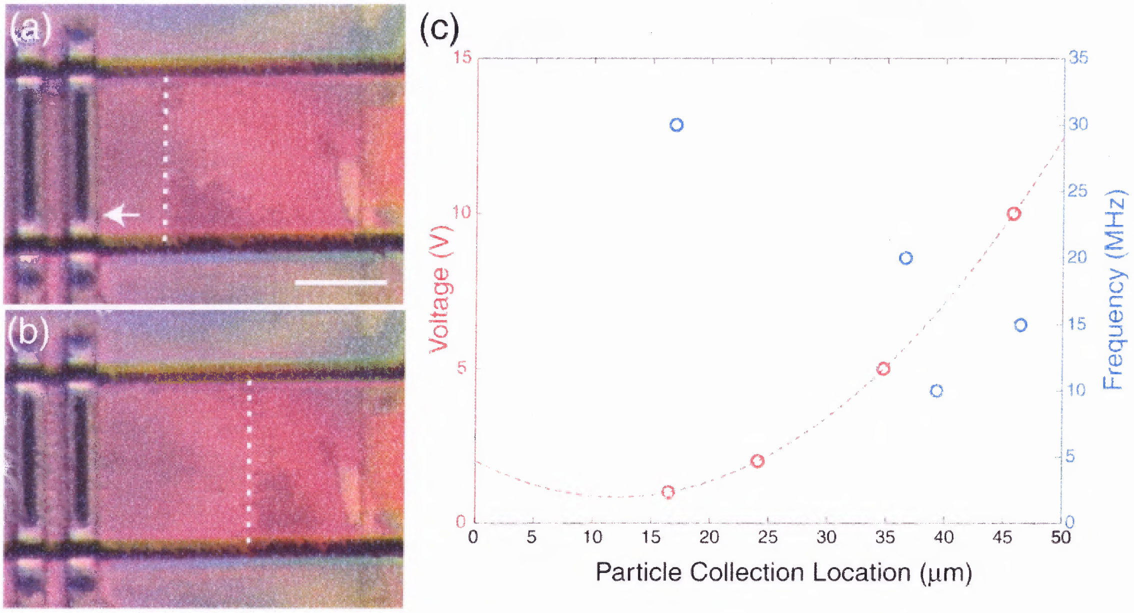

Figure 6.7 DEP of latex particles and Staph. aureus. Fluid flow is from right to left. The electrode (white arrow) is held at (a) 10 V pp, 30 MHz and (b) 10 V pp, 20MHz. Scale bar is 20 μm. Dotted lines indicate the leading edges of collected particles. (c) Dual plot of the horizontal collection location (origin at the electrode) of the latex particles as a function of voltage amplitude and frequency (Graph courtesy of C.D. James, Sandia. National Laboratories).

CHAPTER 7

CONCLUSIONS

A micro-fluidic device equipped with a dielectrophoretic gate has been designed and fabricated using Sandia National Laboratories surface micromachining with integrated fluid technologies process.

Experiments on flowing suspensions of polystyrene latex beads and heat-killed bacteria cells were conducted over a broad range of the particle concentrations and frequencies and voltages of an applied electric field. For high-field frequencies, latex beads exhibit negative dielectrophoresis whereas bacteria cells exhibit positive dielectrophoresis.

It was found that dipolar interactions between particles subject to a high-gradient ac field and shear lead to a new many-body phenomenon of dielectrophoresis accompanied by the field-induced phase separation in a flowing suspension. As a result, shear and electric stresses strongly compress a layer enriched with particles. The predictions of the proposed electro-hydrodynamic model for the coupled shear, dielectrophoresis, and phase separation in a flowing suspension are demonstrated to be consistent with the experiments even though the model contains no fitting parameters.

The study has demonstrated that dielectrophoresis accompanied by the field-induced phase transition provides a powerful method for strongly concentrating particles and for separating biological and non-biological materials flowing through a micro-fluidic device. In this way, substances less polarizable than water (nearly all inorganic materials) can be removed from aqueous solutions.

APPENDIX A

FABRICATION OF TRAVELLING WAVE DEVICES

A.1 Description of Module for Fabrication

The complete module for fabrication consisted of seven different designs of microfluidic channels, Figure A.1. Three of the designs were simple cross like designs measuring 1000 microns in each direction. These designs varied in the spacing of the electrodes with spacings of 5, 10, and 15 microns. This is the spacing of electrodes in the horizontal or x direction. The module also contains a microfluidic channel that is 2000 microns long with a polysilicon teeth-like structure and actuator for splitting particles. In addition, the module contains two single channels of 10 and 15 micron spacing. Finally, the module has a cross-like channel containing posts in the central, cross-sectional region with 10 micron spacing of the posts.

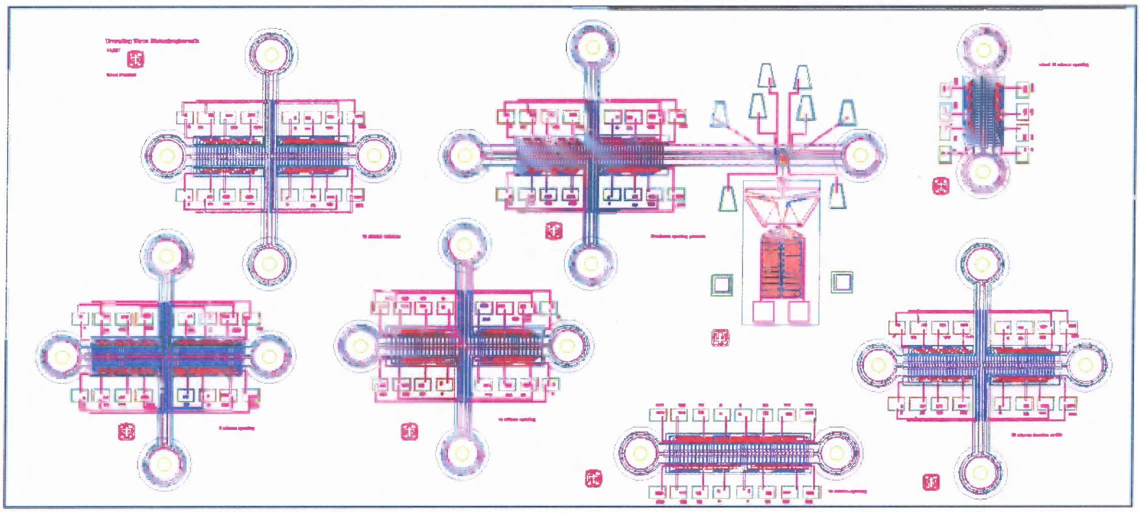

Figure A.1 Module of Microfluidic Channels for Fabrication. Figures show complete masks of module for fabrication. Mask at far left shows plain cross channel of 10 micron spacing; middle top shows longer channel with teeth-like device (Okandan et al., 2001b); top right shows single straight channel; bottom left shows single straight channel 5 micron spacing, 2nd from left bottom shows plain channel 10 micron spacing, 3rd from left bottom shows straight channel; far right bottom shows cross channel with posts.

A.2 Description of Cross Channel

Figures A.2 and A.3 present a diagram of a microfluidic cross-like channel. In the x-direction, the channel measures 16 microns across while the in the y-direction the channel measures 22 microns across. The total length of the channel in each direction is 1000 microns. With the cross channel it is possible to separate two different types of particles into two flow paths. Each channel has sixteen bond pads on each side with different phases applied in order to cause the travelling wave to move down the horizontal channel. The channel is a cross-like channel with 5, 10, and 15 micron spacing between electrodes. This spacing is closer than the spacing in other channels which is typically on the order of tens of micrometers (Wang et al., 1997, Xu et al. 1999, Green et al. 1997).

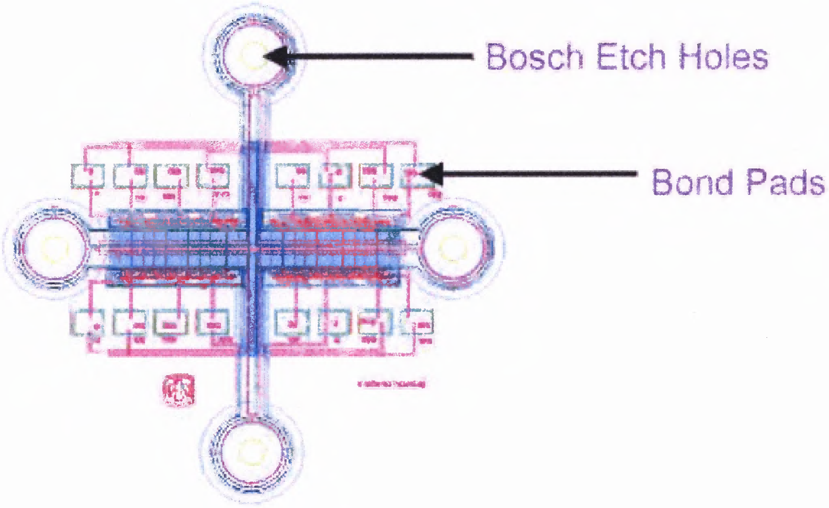

Figure A.2 Mask Layout of a Micromachined Dielectrophoretic Cell Manipulation Device. Figure shows mask of microfluidics cross-channel. Bosched-etched holes are for the inlet and outlet of fluid and suspensions. Bond pads are used for applying electric potential with probes.

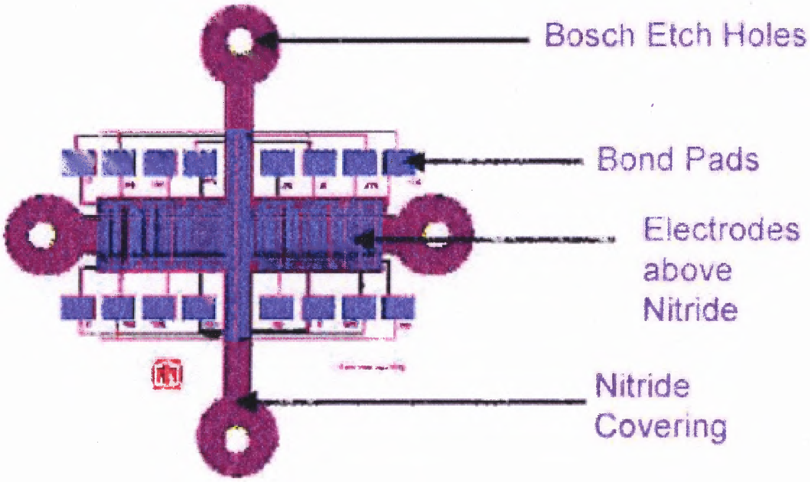

Figure A.3 3-D Visualizer of Microfluidics Channel. Purple shows nitride covering above microfluidic channel. Poly3 electrodes are above nitride covering.

A.3 Cross-Sectional Views of Horizontal Channel

The following Figure A.4 shows a cross-sectional view of the horizontal channel. The blue electrodes on top are made from the third layer of polysilicon (Poly3) layer while the electrodes on the bottom are made from the magenta bottom layer of polysilicon (Poly0). The bottom gray layer is thermal oxide and the dark green is the silicon substrate. The purple layers are nitride deposition and the light blue layer is also nitride deposition. Fluid flows between the electrodes due to a travelling wave caused by varying the phases on the electrodes.

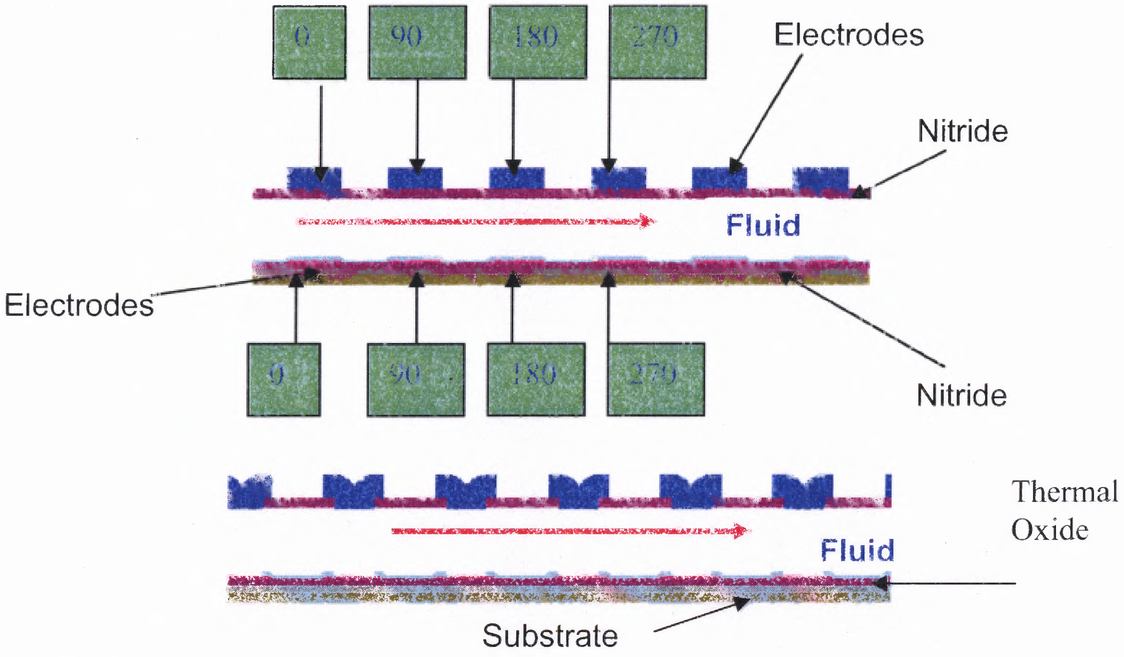

Figure A.4 Cross-Section with top and bottom electrodes. Phases are applied to top and bottom electrodes. Top figure shows electrodes with nitride covering, and bottom figure shows electrodes without nitride covering. The additional nitride covering helps to prevent electrolysis.

Various phases can be applied to each electrode. For example 0, 90, 180, and 270 phase shifts may be applied to the top and bottom electrodes causing the wave to propagate in the horizontal channel. A variety of phase shifts may be applied to vary the sinusoidal pattern of the travelling wave.

The probe tips are applied to the bond pads in Figure A.5. The multilayer SwIFT^{TM} process allows for close spacing of electrodes. On the RHS of Figure A.5 , Poly2 is seen to jump over Poly0. Hence, these two layers of polysilicon will be at different potentials when the field is applied.

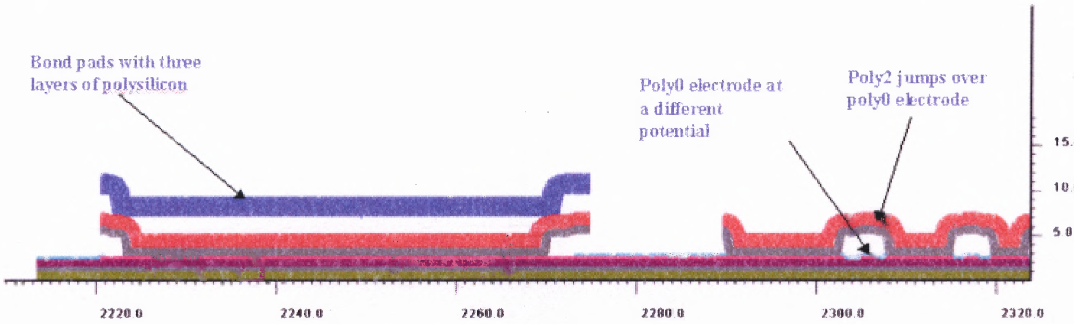

Figure A.5 Cross-section of side of Channel. Bond pads show three layers of polysilicon. Poly2 layer jumps over Poly 0 layer so that these leads are at different potentials. This allows for a close arrangement of electrodes. This is among the closest and smallest electrodes thus far manufactured for travelling wave dielectrophoresis.

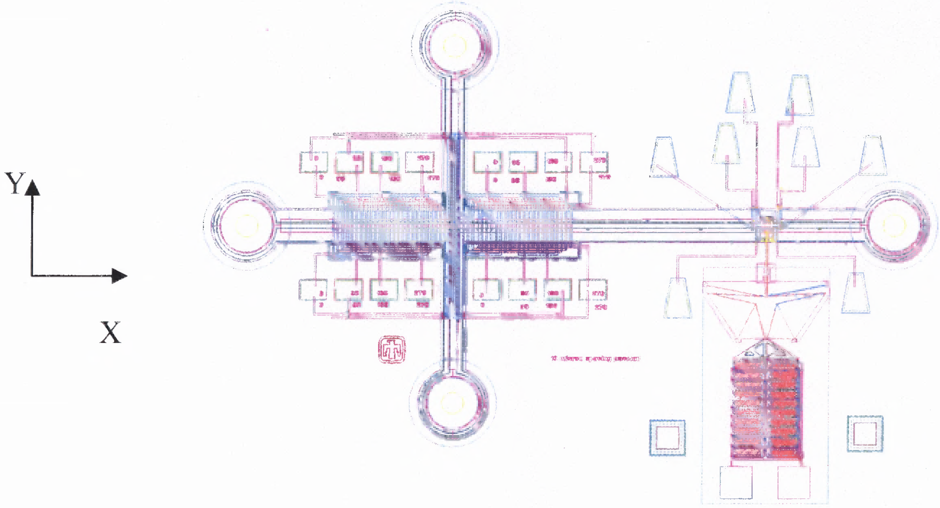

Figure A.6 Mask of long channel with Mechanical Shearing Device. Particles in fluid will come up channel without electrodes and then be captured by travelling wave in channel with electrodes on top and bottom. Particles will then travel down to polysilicon cell splitting device.

The diagram in Figure A.6 above shows the cross-like channel with the mechanical shearig device. Fluid with particles will enter the channel in the Y direction, and the channel in the X direction will carry some of the particles. As the particles move down the horizontal channel, they will be separated and split by the polysilicon teeth-like structure. In this case, etch released holes were placed on each side of the channel because the channel was 2000 microns in length as opposed to the previous length of 1000 microns.

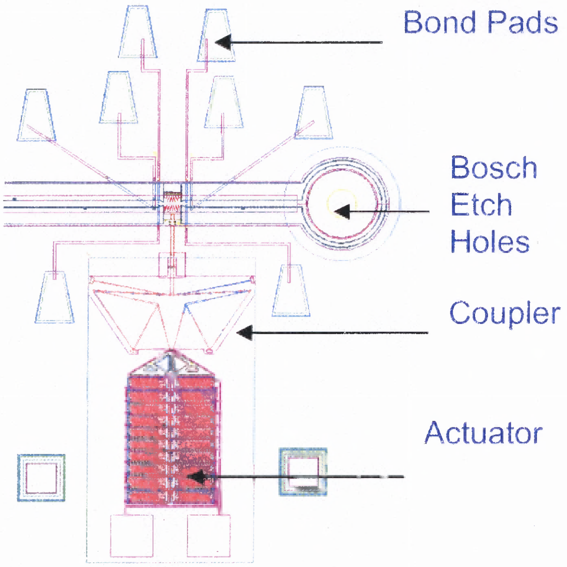

Figure A.7 Mask of Polysilicon cell-splitting device. Coupler and actuator are used to move teeth up and down. Posts are on each side of the mechanical shearing device and bond pads can be used to apply different potentials.

A polysilicon channel with posts in the central region was designed. Posts are shown in Figure A.9. A single horizontal channel as well as a cross-like channel were fabricated with posts. The posts were designed for trapping the electrodes, and they were composed of polysilicon from layers 0, 1, and 2. In addition, single horizontal channels with varied electrode spacing were also fabricated as shown in Figure A.10.

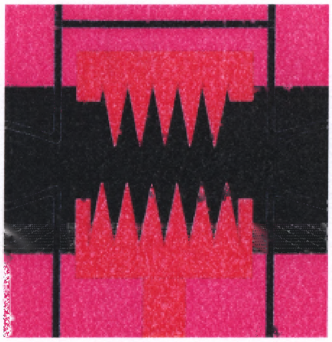

Figure A.8 Mechanical Shearing Device, Polysilicon Teeth.

The mechanical shearing device with polysilicon teeth is shown in a close-up view in Figure A.8. The teeth are interlocking and pointed for splitting or shearing cells. This is an improvement over a previous design in which the teeth were shorter and did not interlock.

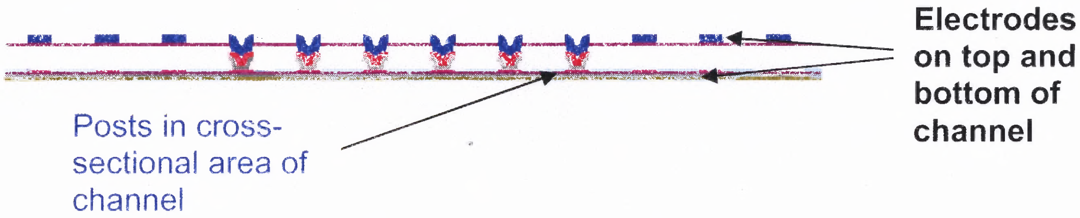

Figure A.9 Cross-Section of Channel with Posts. Cross-section of channel with posts in center region which consist of Poly0, Poly2, and Poly3 electrodes.

Straight channels of 500 μm and 1000 μm in length were also fabricated, Figure A.10. These channels have electrodes on top and bottom, but they only have one inlet and outlet port.

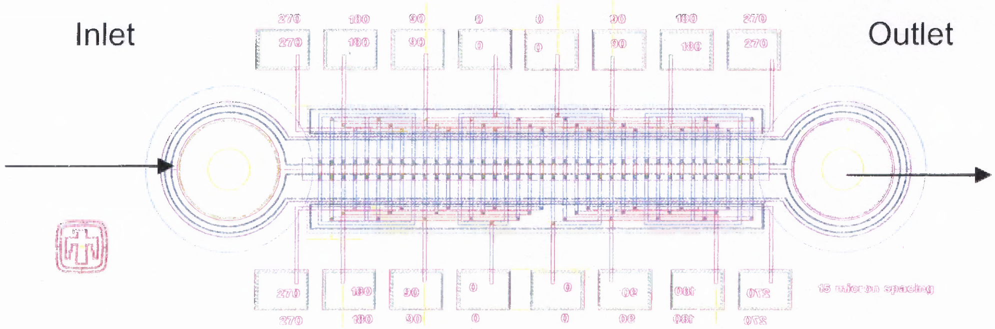

Figure A.10 Single Channel for twDEP 1000 Microns Long.

A second set of designs was made using the SwIFT^{TM} midi process. In this process four layers of polysilicon are used as opposed to five layers in the SwIFT^{TM} process. The lead time for fabrication of these parts is four to five months as opposed to six to eight months in the SwIFT^{TM} process These set of designs are much simpler than the designs for travelling wave dielectrophoresis, because the initial testing and simulations showed that less electrodes are required to establish an electric field gradient. A cross-channel design fabricated using the SwIFT^{TM} midi process is shown in Figure A.11.

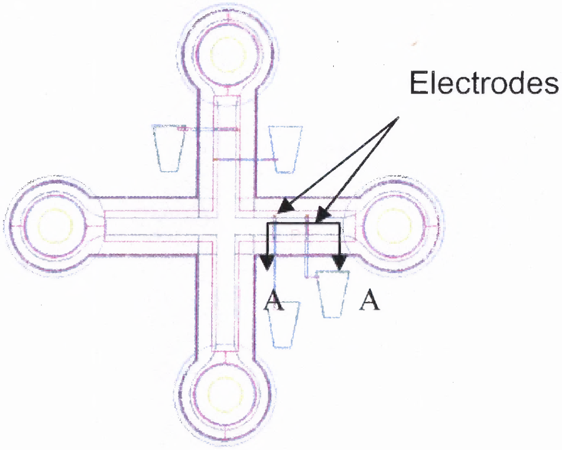

Figure A.11 Close-Up of Channel Designs.

In the SwIFT Midi Process, only two electrodes are used. A sinusoidal ac field will be applied between the electrodes.

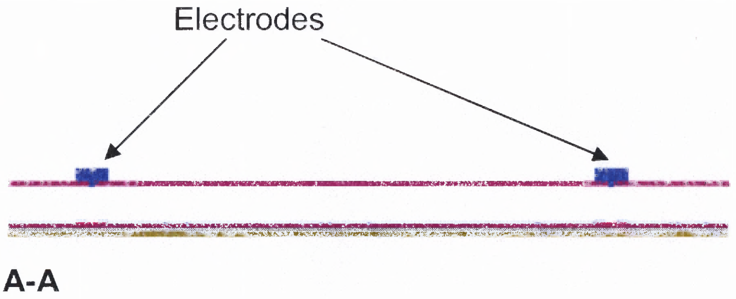

Figure A.12 Cross-Section of Channel with Electrodes.

The design in Figure A.11 contains electrodes on top and bottom for trapping and separating particles in the microfluidics channel. A cross-section is shown if Figure A.12. A mixture of particles can be injected into the channel such as with the SwIFT$^{\text{TM}}$ designs. By manipulating the frequency and voltage, the cells can be trapped by positive dielectrophoresis and the beads can flow around the corners of the electrodes by negative DEP. The beads can also be manipulated to turn in the horizontal channel by varying the voltage on the electrodes in the horizontal channel. Thus, by using conventional dielectrophoresis, it should be possible to cause the cells to be sorted into two different channels.

APPENDIX B

PACKAGING OF MICROFLUIDIC CHANNEL

B.1 Need for a Testing Fixture Channels

One of the problems that arises when working with microfluidic channels is how to get fluid in and out of these channels. This is a problem because of the small size and delicacy of the channels. There is a tendency to blowout the nitride covering of the channel if a high pressure is applied. In addition, there is a problem of leaking. Usually, a non-pulsating Harvard apparatus syringe is used to pump the fluid, and there must be a gradual decrease in size in order for the fluid to be able to pump from the syringe tubing into the channel. Several iterations were made in the development of a testing fixture, and the process is ongoing.

B.2 Testing Fixture for Controlling Fluid Flow

The purpose of the fixture was to enable fluid to be pumped from a syringe pump into microfluidic channels at very high pressures. With the manifold assembly, the maximum pressure that can be obtained is above 14 bars. The first manifold developed was a rectangular acrylic plate with the PEEK part inserted, Figures B.1 and B.2. Fluid was injected into holes in the PEEK part which aligned with holes in the manifold. The PEEK part had tapered channels with smaller holes to mount to the channels on the silicon chip.

B.3 Rectangular Manifold

The silicon part was mounted onto PEEK part using Flip-Chip Bonder device (Figure B.3). The PEEK part was then attached to a rectangular manifold. An outside supplier K-Tech Corporation fabricated the PEEK parts.

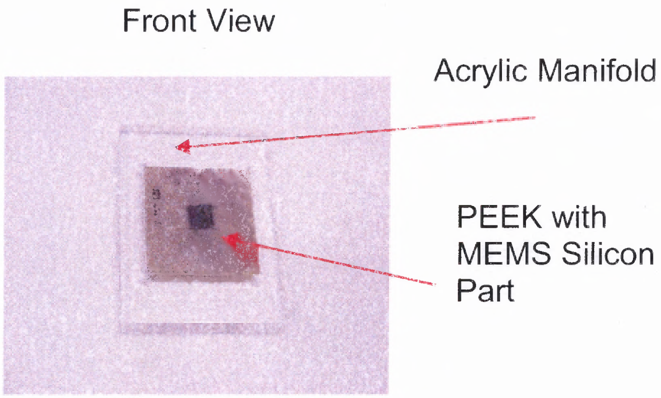

Figure B.1 Rectangular Manifold with PEEK and Silicon Part. Metal tubing was mounted to the rear of the part and fixed with epoxy glue. Fluid would flow into the part from rear, and front view could be viewed with an inverted microscope. High pressures were unable to be obtained because the epoxy glue would often start to leak.

Plastic tubing was attached to the metal connection and fluid was pumped into the larger holes of the rectangular acrylic manifold. The fluid then traveled down the tapered channels until reaching the smaller Bosched-etched hole or inlet port of the microfluidic channel (Figure B.2).

Rear View:

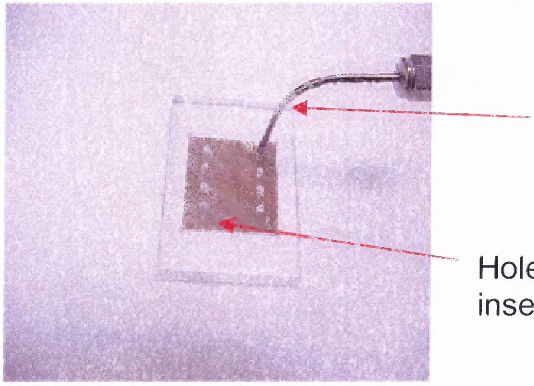

Connection for Tubing

Holes for fluid insertion

Figure B.2 Rear View of Rectangular Manifold and PEEK Part.

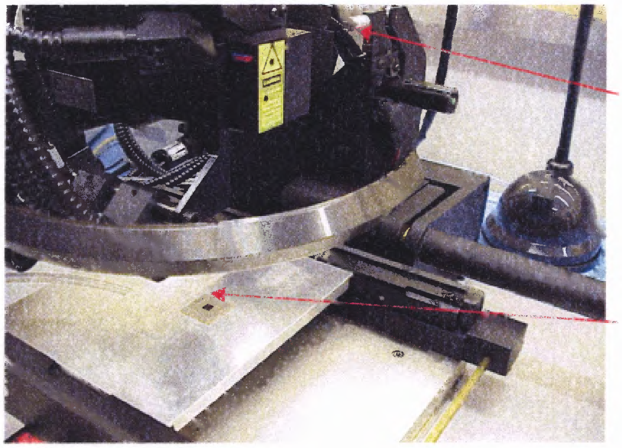

Head mounts down on Silicon Part

Silicon MEMS part mounted onto PEEK part. MEMS part is the target.

Figure B.3 Flip-Chip Bonder for Bonding Silicon Part To PEEK part. The combined silicon and PEEK part are used together with the acrylic manifold for getting fluid into the channels.

The final testing fixture was composed of an acrylic manifold, a rubber gasket, a PEEK part, and steel covering with an aperture, Figures B.4-B.7. Fluid flow into the channels can be viewed from the underside of the manifold. The fluid enters one side of the channel and exits from the other side of the channel. Colored water is used to view the flow pattern.

Between the steel top containing the aperture and the PEEK part is a silicone rubber gasket. The gasket has eight holes close to its outer edge that match up with the eight exterior holes in the PEEK part. In this case, the gasket was manufactured by Industrial Gaskets Corporation of Denver, Colorado. The gasket measures approximately 0.02 microns in thickness and about 0.913 inches along the edge. Gaskets were made from silicone rubber and urethane. It was found that silicone rubber performed the best as far as preventing leakage outside of the channels. A variety of torques were applied; however, it was found torque of 26 in-oz worked best to fasten down the steel plate to the manifold.

B.4 Advantages of the Design

Prior to developing this device it was very difficult to get fluid to go into the microfluidic channels. A capillary tube had to be hand placed into the Bosched-etched holes of the channels. This required an exceptionally good eye and a steady hand. It would sometimes take one half of an hour or more to place the capillary into the microfluidics channel, and afterwards it was very difficult to attach the tubing to the capillary. Many times the capillary tube would just drop out of the channel. Using the new device, the delicacy is eliminated. All that is required is to screw down the steel plate on top of the acrylic manifold. A torque wrench is used for uniform pressure and repeatability. Thus, this is seen as a major improvement over the previous techniques.

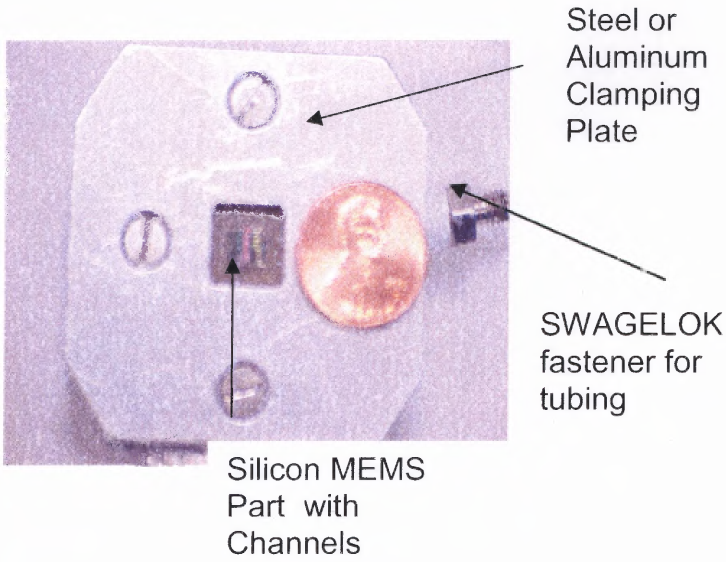

Figure B.4 Top View of Manifold Assembly – Final Assembly.

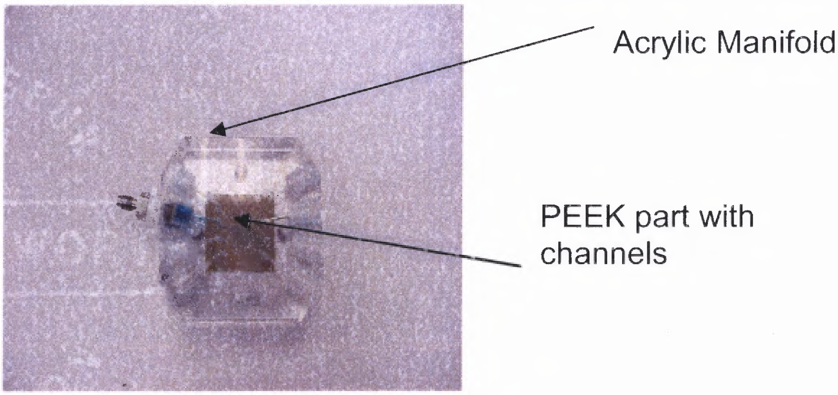

Figure B.5 Rear View of Manifold Assembly.

As part of the manifold assembly, a PEEK part and silicone rubber manifold were designed. The larger end of the channel mated up with the holes in the acrylic plate. While the smaller holes mated up with the Bosched-etched holes in the microfluidic channel.

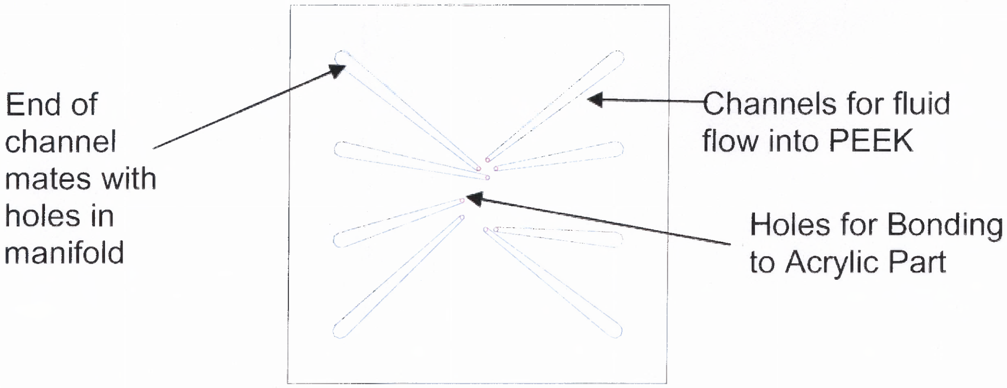

Figure B.6 PEEK Part for Flowing Liquid into Channels (Bottom View).

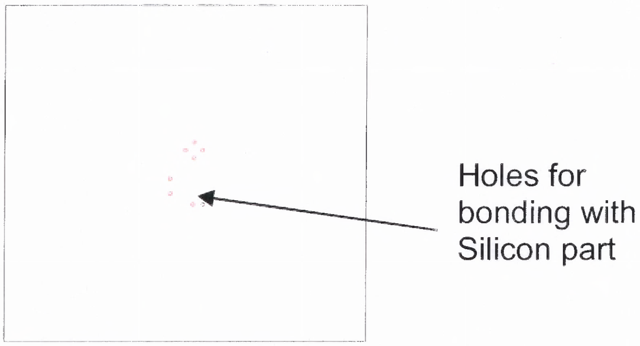

Figure B.7 PEEK PART (Top View).

Another technique involves the use of ultraviolet light and FOTURAN. FOTURAN is a photosensitive glass. This characteristic enables it to be structured for a variety of purposes. The main difference between FOTURAN and ceramic materials is that FOTURAN is pore-free. Its temperature stability and chemical resistance are notably higher than those of plastics. The FOTURAN part is shown if Figure B.8.

www.us.schott.com/tgd/english/products/foturan.html

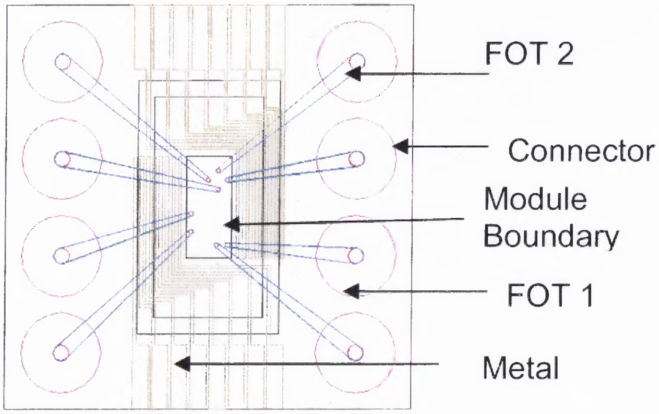

Figure B.8 FOTURAN Part.

In Sandia's designs a couple of layers of FOTURAN would be used, but the procedure would be the same. Figure B.9 shows typical steps in the FOTURAN process.

http://www.design.caltech.edu/micropropulsion/foturane.html

1. UV-Exposure
In the exposure step, FOTURAN® glass is exposed to ultraviolet light at a wavelength between 290 - 330 nm. It is possible to illuminate material thicknesses of up to 2 mm. An energy density of approximately 2 Joule/cm² is sufficient to structurize a 1 mm thick FOTURAN® plate.

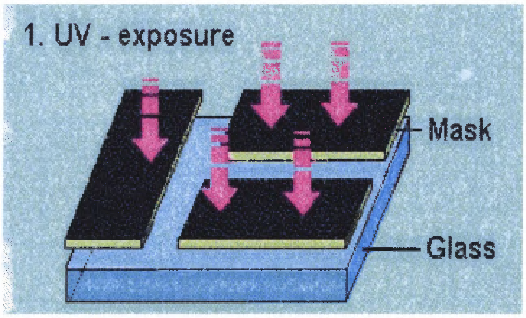

2. Heat treatment
With the UV exposure step silver atoms are formed in the illuminated areas. During the heat treatment between 500° and 600°C the glass crystallizes around these silver atoms.

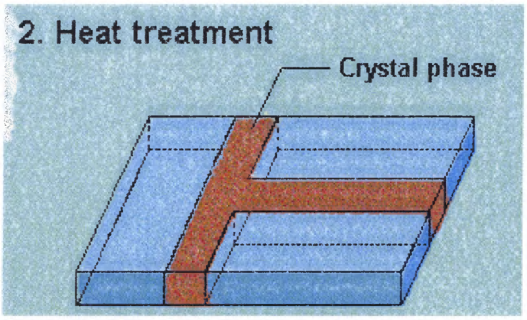

3. Etching

The crystalline regions, when etched with a 10% solution of hydrofluoric acid at room temperature, have an etching rate up to 20 times higher than that of the vitreous regions. If wet chemical etching is supported by ultrasonic etching or by spray etching, the resulting structures display a large aspect ratio.

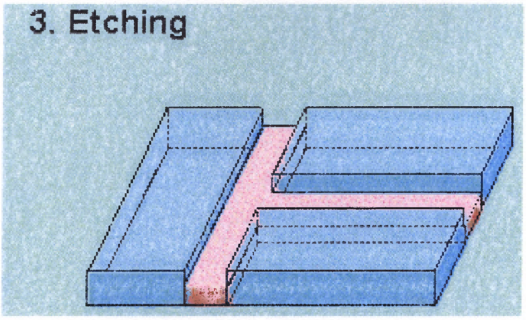

Figure B.9 FOTURAN Procedure Diagram showing three phases of the FOTURAN Procedure: 1 UV Exposure, 2 Heat treatment, and 3 Etching.

REFERENCES

D. Bennett, B. Khusid, P. Galambos, C. D. James, M. Okandan, D. Jacqmin, and A. Acrivos, Combined Field-induced Dielectrophoresis and Phase Separation for Manipulating Particles in Microfluidics, Applied Physics Letters **83** (23), (2003).

S. S. Dukhin and V.N. Shilov, Dielectric Phenomena and the Double layer in Disperse Systems and Polyelectrolytes (Wiley, New York, 1974).

A. Dussaud, B. Khusid, and A. Acrivos, Particle segregation in suspensions subject to high-gradient ac electric fields, Journal of Applied Physics **88**, 5463 (2000).

C. Effenhauser, A. Manz, H.M. Widmer, Glass Chips for High-Speed Capillary Electrophoresis Separations with Submicrometer Plate Heights, Analytical Chemistry **65**, 2637-2642 (1993).

P. C. Galambos, Micromechanical Systems, Principles Of, Encyclopedia of Materials: Science and Technology (Elsevier Science, LTD 2001).

P. R. C. Gascoyne,Y. Huang, R. Pethig, J. Vykoukal, and F. Becker, Dielectrophoretic Separation of Mammalian Cells Studied by Computerized Image Analysis, Measurements Science and Technology, **3**, 439-445, (1992).

P. R. C. Gascoyne and J. Vykoukal, Particle separation by dielectrophoresis, Electrophoresis **23**, 1973 (2002).

S. Habermehl, Stress Relaxation in Si-rich, Silicon Nitride Thin Films, Journal of Applied Physics **83**(9), 4672 (1998).

Handbook of Electrostatic Processes, edited by J.-S. Chang, A.J. Kelly, and J.M. Crowley (Marcel Dekker, New York, 1995).

K. C. Hass, Computer simulations of nonequilibrium structure formation in electrorheological fluids, Physical Review E **47**, 3362 (1993).

A. Heller, BASIS Counters Airborne Bioterrrorism, Science and Technology, (October 2003).

M. P. Hughes, R. Pethig, and X.B,,Wang, Dielectrophoretic forces on particles in Travelling Electric Fields, Journal of Physics D: Applied Physics **29**, 474-482 (1996).

M. P. Hughes, AC Electrokinetics: Applications in Nanotechnology, Seventh Foresight Conference on Molecular Nanotechnology (1999, November 30).

T. B. Jones, Electromechanics of Particles (Cambridge University Press, Cambridge, 1995).

B. Khusid and A. Acrivos, Effects of conductivity in electric-field-induced aggregation in electrorheological fluidics, Physical Review E **52**, 1669 (1995).

B. Khusid and A. Acrivos, Phase diagrams of electric-field-induced aggregation in conducting colloidal suspensions, Physical Review E **60**, 3015 (1999).

B. Khusid and A. Acrivos, Effects of Interparticle Electric Interactions on Dielectrophoresis of Colloidal Suspensions, Physical Review E **54**, 5428 (1996).

M. Koch, A. Evans, and A. Brunnschweiler, Microfluidic Technology and Applications (Research Studies Press, Baldock, 2000).

L. D. Landau, E.M. Lifshitz, and L.P. Pitaevski, Electrodynamics of Continuous Media (Pergamon, Oxford, 1984).

N. Markarian, M. Yeksel, B. Khusid, K. Farmer, and A. Acrivos, Limitations on the scale of an electrode array for trapping particles in microlfuidics by positive dielectrophoresis, Applied Physics Letters, **82,** 4839 (2003).

D. R. Meldrum and M.R. Holl, Microscale bioanalytical systems, Science, **297**, 1197 (2002).

M. Okandan, P. Galambos, S.S. Mani, and J. Jakubczak, Development of Surface Micromachining Technologies for Microfluidics and BioMEMS, SPIE Microfluidics and BioMEMS 2001, Proceedings of SPIE, vol 4560 2001(a) 113-139.

M. Okandan, P. Galambos, S.S. Mani, and J. Jakubczak, Surface Micromachined Cell Manipulation Device for Transfection and Sample Preparation, Micro Total Analysis Systems 2001(b), 305-306.

J. Ouellette, A new wave of microfluidic devices, Industrial Physicist **9**,14 (2002).

H. A. Pohl, Dielectrophoresis: The Behavior of Neutral Matter in Nonuniform Electric Fields (Cambridge University Press, Cambridge, 1978).

B. Russel, D.A. Saville, and W.R. Schowalter, Colloidal Dispersions (Cambridge University Press, Cambridge, 1989).

M. Shapiro, A.L. Shalom, and I.J. Lin, Dielectric flocculation of nondiffusive particles in a nonconducting fluid and a uniform electric field, Journal of Applied Physics **58**, 1028 (1985).

J. Sniegowski and M. De Boer, IC-compatible polysilicon surface micromachining, Annual Review Materials Science **30**, 299-333 (2002).

H. A. Stone and S. Kim, Microfluidics: Basic issues, applications and challenges. American Institute of Chemical Engineers Journal **47**, 1250 (2001).

A. Terray, J.Oakey, and D.Marr, Microfluidic Control Using Colloidal Devices, Science, **296**, 1841-1843 (June 2002).

Z. Qiu, N. Markarian, B. Khusid, and A. Acrivos, Positive dielectrophoresis and heterogeneous aggregation in high-gradient ac electric fields, Journal of Applied Physics **92**, 2829 (2002).

M. Ungarish, Hydrodynamics of Suspensions (Springer-Verlag, Berlin, 1993).

G. M. Whitesides, Stroock, Flexible Methods for Microfluidics,_Physics Today, **54**, 42, (June 2001).